



# Impact of Stellar Superflares on Planetary Habitability

Yosuke A. Yamashiki<sup>1,2</sup>, Hiroyuki Maehara<sup>3,4</sup>, Vladimir Airapetian<sup>5,6</sup>, Yuta Notsu<sup>7,8,9</sup>, Tatsuhiko Sato<sup>10</sup>, Shota Notsu<sup>9,11</sup>, Ryusuke Kuroki<sup>1</sup>, Keiya Murashima<sup>12</sup>, Hiroaki Sato<sup>13</sup>, Kosuke Namekata<sup>9</sup>, Takanori Sasaki<sup>2,9</sup>, Thomas B. Scott<sup>14</sup>, Hina Bando<sup>12</sup>, Subaru Nashimoto<sup>12</sup>, Fuka Takagi<sup>15</sup>, Cassandra Ling<sup>1</sup>, Daisaku Nogami<sup>2,9</sup>, and Kazunari Shibata<sup>2,16</sup>

<sup>1</sup> Graduate School of Advanced Integrated Studies in Human Survivability, Kyoto University, Sakyo, Kyoto, Japan; [yamashiki.yosuke.3u@kyoto-u.ac.jp](mailto:yamashiki.yosuke.3u@kyoto-u.ac.jp)

<sup>2</sup> Unit of the Synergetic Studies for Space, Kyoto University, Sakyo, Kyoto, Japan

<sup>3</sup> Okayama Branch Office, Subaru Telescope, National Astronomical Observatory of Japan, NINS, Kamogata, Asakuchi, Okayama, Japan

<sup>4</sup> Okayama Observatory, Kyoto University, Kamogata, Asakuchi, Okayama, Japan

<sup>5</sup> NASA/GSFC/SEEC, Greenbelt, MD, USA

<sup>6</sup> American University, Washington, DC, USA

<sup>7</sup> Laboratory for Atmospheric and Space Physics, University of Colorado Boulder, Boulder, CO, USA

<sup>8</sup> National Solar Observatory, Boulder, CO, USA

<sup>9</sup> Department of Astronomy, Kyoto University, Sakyo, Kyoto, Japan

<sup>10</sup> Nuclear Science and Engineering Center, Japan Atomic Energy Agency (JAEA), Tokai, Ibaraki, Japan

<sup>11</sup> Leiden Observatory, Leiden University, Leiden, The Netherlands

<sup>12</sup> Faculty of Science, Kyoto University, Sakyo, Kyoto, Japan

<sup>13</sup> Faculty of Engineering, Kyoto University, Sakyo, Kyoto, Japan

<sup>14</sup> Interface Analysis Centre, University of Bristol, Bristol, UK

<sup>15</sup> Faculty of Agriculture, Kyoto University, Sakyo, Kyoto, Japan

<sup>16</sup> Astronomical Observatory, Kyoto University, Sakyo, Kyoto, Japan

Received 2019 April 17; revised 2019 June 12; accepted 2019 June 16; published 2019 August 20

## Abstract

High-energy radiation caused by exoplanetary space weather events from planet-hosting stars can play a crucial role in conditions promoting or destroying habitability in addition to the conventional factors. In this paper, we present the first quantitative impact evaluation system of stellar flares on the habitability factors with an emphasis on the impact of stellar proton events. We derive the maximum flare energy from stellar star spot sizes and examine the impacts of flare-associated ionizing radiation on CO<sub>2</sub>, H<sub>2</sub>, and N<sub>2</sub>+ O<sub>2</sub>-rich atmospheres of a number of well-characterized terrestrial type exoplanets. Our simulations based on the Particle and Heavy Ion Transport code System suggest that the estimated ground-level dose for each planet in the case of terrestrial-level atmospheric pressure (1 bar) for each exoplanet does not exceed the critical dose for complex (multicellular) life to persist, even for the planetary surface of Proxima Centauri b, Ross-128 b, and TRAPPIST-1 e. However, when we take into account the effects of the possible maximum flares from those host stars, the estimated dose reaches fatal levels at the terrestrial lowest atmospheric depth on TRAPPIST-1 e and Ross-128 b. Large fluxes of coronal X-ray and ultraviolet radiation from active stars induce high atmospheric escape rates from close-in exoplanets, suggesting that the atmospheric depth can be substantially smaller than that on Earth. In a scenario with the atmospheric thickness of one-tenth of Earth's, the radiation dose from close-in planets including Proxima Centauri b and TRAPPIST-1 e reaches near fatal levels with annual frequency of flare occurrence from their host stars.

**Key words:** planet–star interactions – solar–terrestrial relations – stars: flare – Sun: coronal mass ejections (CMEs) – sunspots

## 1. Introduction

The definition of habitable zones for extrasolar planetary systems is traditionally based on the conditions promoting the presence of standing bodies of liquid surface water (determined to be a conventional habitable zone [CHZ]), but other more refined boundaries may be considered (Kopparapu et al. 2013; Ramirez et al. 2019). For example, the inner habitable boundary may be defined by critical fluxes, which cause runaway/moisture greenhouse effects (Kasting 1988), while the outer boundary may be constrained by the presence of carbon dioxide in the atmosphere in the gas phase, avoiding its condensation (Kasting et al. 1993). The exoplanets within CHZs around active stars can be subject to high ionizing radiation fluxes including X-ray and extreme ultraviolet emission (referred as to XUV [1–1200 Å] emission), coronal mass ejections (CMEs), and associated stellar energetic particles (SEP) events that can affect exoplanetary habitability conditions (Airapetian et al. 2017a; Airapetian et al. 2019).

Energetic stellar flare events associated with CMEs from magnetically active stars can contribute to the generation of stellar transient XUV emission and form high-energy particles accelerated in CME-driven shocks (Gopalswamy et al. 2017; Kumari et al. 2017; Airapetian et al. 2019). These SEPs can penetrate into exoplanetary atmospheres and cause chemical changes. These changes can be positive for the initiation of prebiotic chemistry in the planetary atmospheres or detrimental due to the destruction of a large fraction of ozone that transmits UVC (1000–2800 Å) and UVB (2800–3150 Å) emission to the exoplanetary surfaces (Segura et al. 2010; Airapetian et al. 2016, 2017b; Tilley et al. 2019).

Our own Sun is known to exhibit extreme flare activity in the past, including the so-called Carrington-class event (Townsend et al. 2006). Recent observations by the *Kepler* space telescope revealed that young solar-type stars generate a much higher frequency of energetic flares (superflares), which could have been an important factor for habitability in the early history of our solar

**Table 1**  
Basic Parameters of Target Planets and Their Host Stars, Including Their Projected Flare Energy

Exoplanet Name	Planet			Host Star					Flare Energy (erg)	
	Radius ( $R_{\text{Earth}}$ )	Size Class	Mass ( $M_{\text{Earth}}$ )	Spectra Type	$T_{\text{eff}}$ (K)	Radius ( $R_{\odot}$ )	$P_{\text{rot}}$ (days)	$A_{\text{spot,p}}/(2\pi R_{\odot})$	Annual	Spot Maximum
GJ 699 b	1.37	super-Earth-size	3.23	M4V	3278	0.18	140.0	0.0003	6.26E+31	1.15E+32
Kepler-283 c	1.82	super-Earth-size	4.59	K5	4141	0.64	18.2	0.0021	4.93E+32	2.13E+33
Kepler-1634 b	3.19	Neptune-size	7.77	G7	5637	0.82	19.8	0.0066	1.65E+33	1.18E+34
Proxima Centauri b	1.07	Earth-size	1.27	M5.5V	3050	0.14	82.6	0.0040	9.7E+32	5.55E+33
Ross-128 b	1.10	Earth-size	1.40	M4	3192	0.20	121.0	0.0002	4.72E+31	7.72E+31
TRAPPIST-1 b	1.09	Earth-size	0.86	M8	2550	0.12	3.3	0.0012	2.70E+32	9.09E+32
TRAPPIST-1 c	1.06	Earth-size	1.38	M8	2550	0.12	3.3	0.0012	2.70E+32	9.09E+32
TRAPPIST-1 d	0.77	Earth-size	0.41	M8	2550	0.12	3.3	0.0012	2.70E+32	9.09E+32
TRAPPIST-1 e	0.92	Earth-size	0.64	M8	2550	0.12	3.3	0.0012	2.70E+32	9.09E+32
TRAPPIST-1 f	1.05	Earth-size	0.67	M8	2550	0.12	3.3	0.0012	2.70E+32	9.09E+32
TRAPPIST-1 g	1.13	Earth-size	1.34	M8	2550	0.12	3.3	0.0012	2.70E+32	9.09E+32
TRAPPIST-1 h	0.76	Earth-size	0.36	M8	2550	0.12	3.3	0.0012	2.70E+32	9.09E+32
Sol d (Earth)	1.00	Earth-size	1.00	G2V	5778	1.00	25.0	0.0030	7.20E+32	3.64E+33
Sol e (Mars)	0.53	Mars-size	0.11	G2V	5778	1.00	25.0	0.0030	7.2E+32	3.64E+33

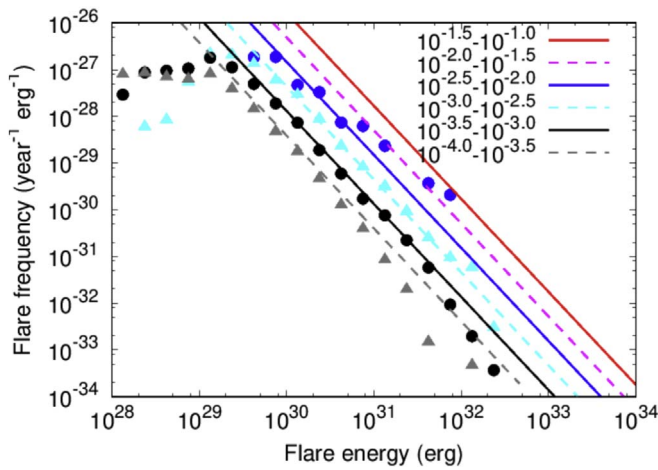


**Figure 1.** Flare frequency vs. flare energy for solar flares. The fraction of flare stars as a function of the rotation period. The solid line and dotted line represent the estimated scaling law calculated using Equation (1) as different star spot areas derived from Maehara et al. (2017).

system and/or most extrasolar systems (Maehara et al. 2012; Shibayama et al. 2013; Takahashi et al. 2016; Notsu et al. 2019; Airapetian et al. 2019). Extreme surges of  $^{14}\text{C}$  were detected in tree rings (Miyake et al. 2012, 2013), which is considered strong evidence of the occurrence of superflares more than one magnitude stronger than the Carrington-class event (Usoskin et al. 2013). Effects of stellar activity from host stars may also include periodic sterilizing doses of radiation via stellar superflare activity (Lingam & Loeb 2017). While the frequency and maximum energy of solar and stellar flares from planet hosts have not been well characterized, they may present a critical limiting factor on the development and persistence of life on terrestrial-type planets in our solar system (Jakosky et al. 2015; Schrijver et al. 2015; Kay et al. 2016) as well as on Earth-sized exoplanets (Atri 2017). Thus, a consistent approach to determine the habitable zone accounting for these factors is required. The characterization of these factors can be made using a recently derived correlation between stellar flare frequency/intensity and star spot area, found from *Kepler* data, which may overcome the difficulty in predicting a flare-impacted system (Maehara et al. 2017).

Here we present the first comprehensive impact evaluation system of expected ground-level radiation doses in close-in terrestrial-type exoplanets around M dwarfs including Proxima Centauri b (see Table 1) in response to severe solar proton events (SPEs). This study represents a realistic model of the surface dose evaluation for exoplanets with various possible atmospheric pressures and compositions. Section 1 presents the framework for evaluation of SPE particle fluence at the top of exoplanetary atmospheres. In Section 2 we discuss the application of the Particle and Heavy Ion Transport code System (PHITS) to a number of close-in exoplanets around M dwarfs. Section 3 discusses the ground dose for various exoplanetary systems and their consequences for the biological habitability of complex life-forms. Section 4 describes the conclusions of the paper and future work.

## 2. Method

### 2.1. Outline of Fluence Estimation for Top of Atmosphere (TOA) on Each Planet from Stellar Proton Events and Definition of Maximum Flare Energy

Our analysis is based on the application of stellar flare and star spot data derived mostly from the *Kepler* mission (Notsu et al. 2013, 2015a, 2015b, 2019; Maehara et al. 2015, 2017), in the ExoKyoto exoplanetary database (Y. A. Yamashiki et al. 2019, in preparation). Our method utilizes star spot data derived from optical light curves to be used in parametric studies of the thickness of hypothetical exoplanetary atmospheres as the major attenuation factor of the incident radiation (see Table 1). These data are used as input for the PHITS (Sato et al. 2018) Monte Carlo simulation model that is used for simulations of surface dose for terrestrial-type exoplanets.

The following equations derive an assumed stellar flare magnitude from observed stellar spot size data. For the estimation of spot size, we used the same method as Maehara et al. (2017). Figures 1 and 2 illustrate flare frequency versus flare energy for solar flares. The solid line and dotted line represent the estimated scaling law calculated using Equation (1) as a different star spot area derived from Maehara et al. (2017).

Using the results of the above study, we derived the flare frequency distribution over its energy in the optical band as a

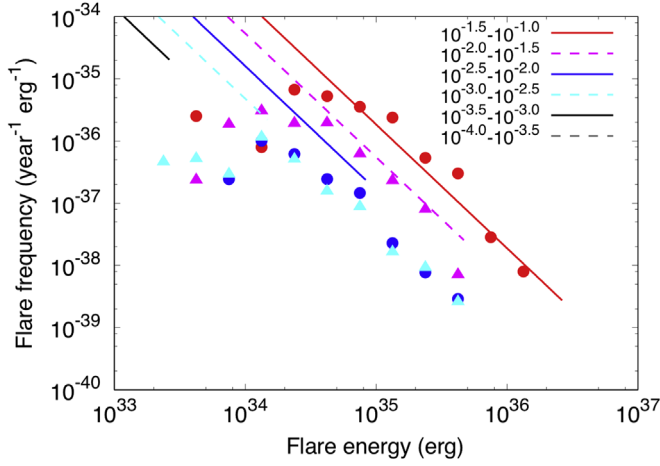


**Figure 2.** Flare frequency vs. flare energy for stellar flare. The fraction of flare stars as a function of the rotation period. The solid line and dotted line represent the estimated scaling law calculated using Equation (1) as different star spot areas derived from Maehara et al. (2017).

function of the stellar spot size as follows:

$$\frac{dN}{dE} = C_0 [\text{yr}^{-1} \text{erg}^{-1}] \left[ \frac{A_{\text{spot}}}{10^{-2.75} A_{\text{phot}}} \right]^{1.05} \left[ \frac{E_{\text{flare}}}{10^{31} \text{erg}} \right]^{-1.99}, \quad (1)$$

in which  $N$  is the flare frequency ( $\text{yr}^{-1}$ ),  $A_{\text{spot}}$  is the total area of star spots,  $A_{\text{phot}}$  is the total visible area of the stellar surface,  $E_{\text{flare}}$  is the total expected stellar flare energy (erg), and  $C_0$  is the flare frequency constant ( $10^{29.4}$ ).

Here we define  $E_0 = 10^{31}$  erg and set  $N$  as 1; we then may determine annual maximum flare energy as follows:

$$E_{\text{AMF}} = C_0^{-\frac{1}{1+a}} \left[ \frac{A_0}{A} \right]^{\frac{b}{1+a}} E_0^{\frac{a}{1+a}}, \quad (2)$$

in which  $E_{\text{AMF}}$  is the annual maximum flare energy, that is, the total expected stellar flare energy per year ( $\text{erg yr}^{-1}$ ),  $a = -1.99$ ,  $b = 1.05$ .

The spot maximum flare, that is, the maximum flare energy under a determined star spot area, can be illustrated as

$$E_{\text{SMF}} = 7 \times 10^{32} (\text{erg}) \left( \frac{f}{0.1} \right) \left( \frac{B_0}{10^3 \text{G}} \right)^2 \left[ \frac{A_{\text{spot}} / (2\pi R_{\odot}^2)}{0.001} \right]^{3/2}, \quad (3)$$

in which  $f$  is the fraction of magnetic energy that can be released as flare energy,  $B$  is the magnetic field strength,  $E_{\text{SMF}}$  is the spot maximum flare energy, that is, the theoretical maximum flare energy with a determined star spot area (erg), and  $R_{\odot}$  is the solar radius ( $7 \times 10^{10}$  cm).

Possible maximum flare energy in this study was determined in the following way: (1) Evaluate maximum star spot coverage of the star through observation of stellar light curves. In this study, we observed a 20% coverage of star spot on Proxima Centauri (Davenport 2016; Wargelin et al. 2017); accordingly we determined the maximum star spot coverage as 20%. Then, (2) calculate maximum energy induced by the star spot area by Shibata et al. (2013).

The outline of the estimation method is as follows:

Step 1. Derive the magnitude and frequency of stellar proton events from each star (1) by using direct observation of a stellar

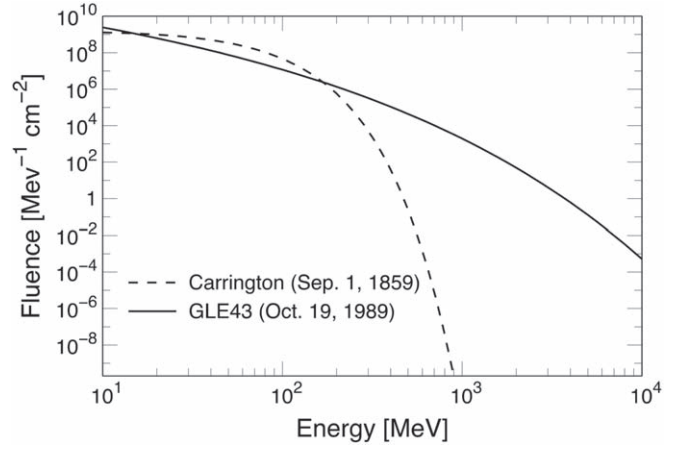


**Figure 3.** Event-integrated spectra, of the GLE43 that occurred on the 1989 October 19 (solid line) and the Carrington flare that occurred on the 1859 September 1 (dotted line) SPEs on Earth, based on parameters obtained from references.

flare as a proxy for SPE energy and (2) by applying the star spot area and/or rotational period correlation methodology. The conversion equation is presented and discussed in the next section. We use the above information to extract representative star spot areas, which can be applied to the conversion equations for flare energy expressed in the following section. Accordingly we obtain (a) annual maximum flare (see Equation (2)), spot maximum flare (see Equation (3)) (Shibata et al. 2013; Aschwanden et al. 2017), and (c) possible maximum flare, calculated assuming that the target star surface is covered with star spots under the maximum percentage of observed star spot area (set as 20% of half the spherical area).

Step 2. After the above procedure is completed for each star system, the possible quantitative exposures are assumed by the following procedure: (4) estimating the fluence of each stellar proton event at the TOA using Equation (7).

As for the atmospheric compositions of exoplanets, three types of atmospheres for typical extrasolar planets are considered (explained in detail in the following section). For those typical atmospheric compositions, the potential doses for life on extrasolar planets are determined through the following procedure.

Step 3. (5) Calculate the possible dose rate from the Monte Carlo simulations using PHITS (Sato et al. 2018) for three typical atmospheric compositions as extrasolar planetary atmospheres, (6) normalize the dose by determining the Earth equivalent ratio, which was previously normalized by using (6a) the Carrington-class event, assuming that the event has X45 class, or by (6b) the deepest observed flare event GLE43, which occurred in 1989, as X13 class (Xapsos et al. 2000). (7) Calculate conversion coefficients for each exoplanet by comparing the values calculated in (4) and (6). (8) Convert the reference dose value calculated in (6) into each extrasolar planet case using conversion coefficients.

## 2.2. Monte Carlo Simulation for Air Shower Using PHITS

When high-energy SEPs precipitate into the planetary atmosphere, they induce extensive air shower (EAS) by producing various secondary particles, such as neutrons and muons. We conducted a three-dimensional EAS simulation by using the PHITS (Sato et al. 2018), which is a general purpose Monte Carlo code for analyzing the propagation of radiation in

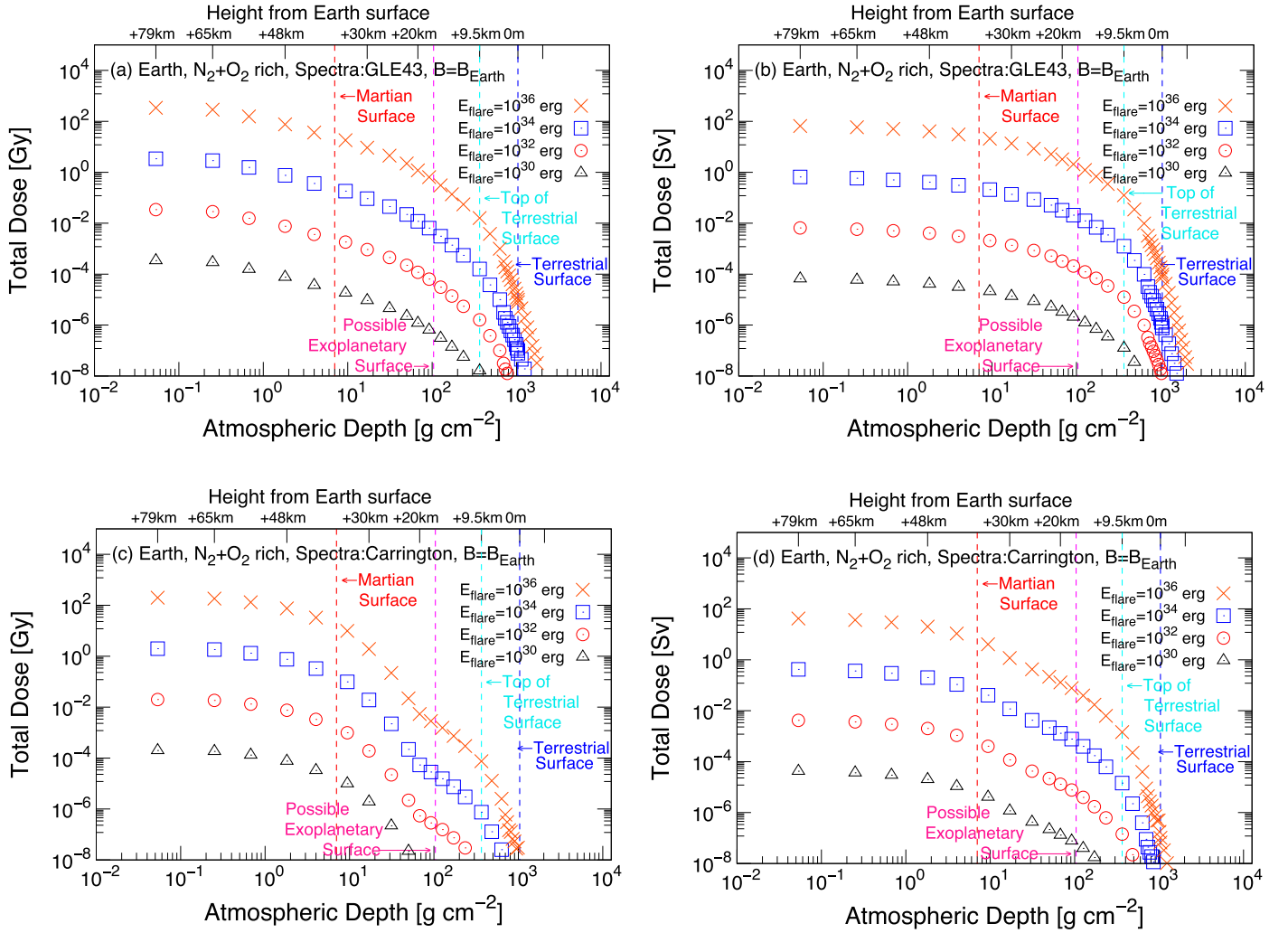


**Figure 4.** Vertical profile of radiation dose on Earth for normalized flares, caused by hard proton spectrum (imitating GLE43) (a and b) and soft spectrum (imitating Carrington by Townsend) (c and d) penetrating  $\text{N}_2 + \text{O}_2$ -rich (terrestrial type) atmosphere for Earth with  $10^{30}$  erg (black triangle),  $10^{32}$  erg (red circle),  $10^{34}$  erg (blue square), and  $10^{36}$  erg (red cross) in grays (a and c) and Sieverts (b and d). The vertical legend shows the following four typical atmospheric depth reference layers: Martian surface atmospheric pressure equivalent to  $9 \text{ g cm}^{-2}$ , terrestrial minimum atmospheric pressure, observed at the summit of the Himalayas, equivalent to  $365 \text{ g cm}^{-2}$  in this study, and (Earth's) ground-level atmospheric pressure, equivalent to  $1037 \text{ g cm}^{-2}$ . Possible exoplanetary surface was estimated as one-tenth of terrestrial surface, equivalent to  $103.7 \text{ g cm}^{-2}$ . Note that the value is not identical to the real observation data but is the nearest value employed in the Monte Carlo numerical simulation using PHITS.

any materials. PHITS version 2.88 with the recommended setting for cosmic-ray transport simulation (Sato et al. 2014) was used in this survey. In our simulations we assume the size and the mass of the modeled planets to be the same as that of the Earth.

### 2.3. Chemical Composition of Exoplanetary Atmospheres

The impact of stellar proton events on a planet depends upon its atmospheric composition. We consider three: Earth-like ( $\text{N}_2 + \text{O}_2$  rich), Mars-like or Venus-like ( $\text{CO}_2$  rich), and a young Earth-sized or super-Earth planet with a primary  $\text{H}_2$ -rich atmosphere. We assume that the Earth-type atmosphere is the standard land-ocean planetary atmosphere composed mostly of nitrogen and oxygen ( $\text{N}_2 + \text{O}_2$ ). A Venusian-like atmosphere is represented as a  $\text{CO}_2$ -rich atmosphere resulting from the runaway greenhouse effect and subsequent outgassing of  $\text{CO}_2$  from carbonates. The Mars-like atmosphere is an example of a low gravity-low pressure planetary  $\text{CO}_2$ -rich atmosphere that

has experienced severe atmospheric escape driven by strong stellar ionizing radiation flux. We also model a young Earth-sized  $\text{H}_2$ -rich atmosphere, because such an atmosphere is assumed for large super-Earth planets, whose gravitational pull might be sufficiently large to retain substantial atmospheric  $\text{H}_2$ . Hydrogen-rich atmospheres of Earth-sized exoplanets can be formed due to capture of hydrogen from protoplanetary atmospheres and/or during the accretion period (Elkins-Tanton & Seager 2008; Lammer et al. 2018). Thus, here we refer to young Earth-sized exoplanets.

The composition of the atmosphere for the above three typical atmospheric types was set to 78% nitrogen, 21% oxygen, and 1% argon for the Earth-like ( $\text{N}_2 + \text{O}_2$ ) atmosphere, 100% carbon dioxide for the Martian/Venusian-type ( $\text{CO}_2$ ), and 100% hydrogen for the young-Earth-type ( $\text{H}_2$ ). During the Monte Carlo simulation using PHITS, we assume the composition of the planet interior to be covered with sufficient liquid water for the terrestrial type, while the same gas was



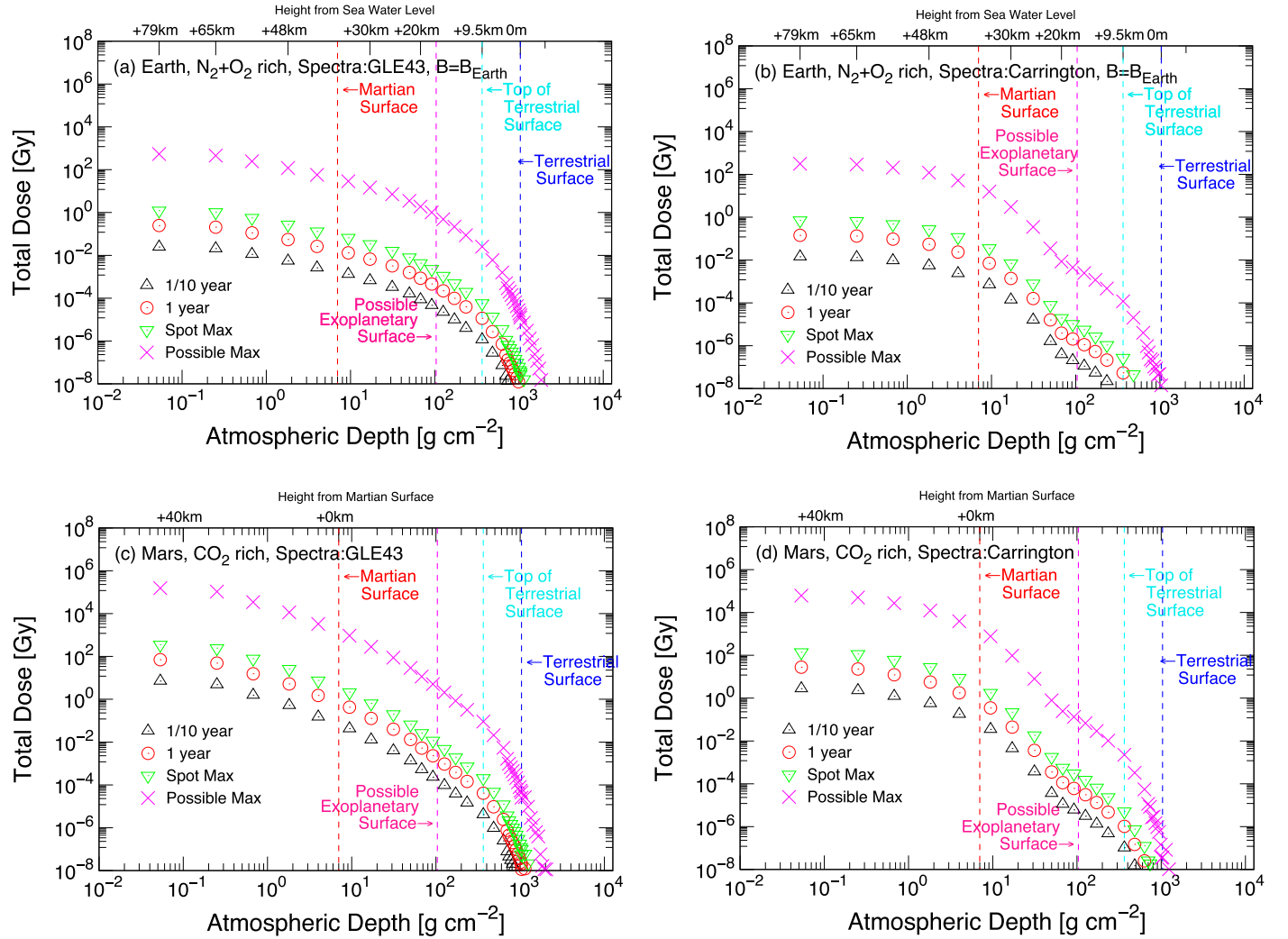


**Figure 5.** Vertical profile of radiation dose (in grays) on Earth and Mars for possible flares on several different scales, caused by hard proton spectrum (imitating GLE43) (a and c) and soft spectrum (imitating Carrington) (b and d) penetrating  $N_2 + O_2$ -rich (terrestrial type) atmosphere for Earth (a and b) and  $CO_2$ -rich (Martian type) atmosphere for Mars (c and d) with flares every one-tenth of a year (36 days, black triangle), one year (red circle), spot maximum (green triangle), and possible maximum (red cross). Martian surface atmospheric pressure is equivalent to  $9 \text{ g cm}^{-2}$ ; terrestrial minimum atmospheric pressure, observed at the summit of the Himalayas, is equivalent to  $365 \text{ g cm}^{-2}$ ; (Earth's) ground-level atmospheric pressure is equivalent to  $1037 \text{ g cm}^{-2}$ ; possible exoplanetary surface is one-tenth of the terrestrial surface, equivalent to  $103.7 \text{ g cm}^{-2}$ .

continuously filled in the planet interior for the other cases. In our simulation of all model atmospheres (young Earth-type  $[H_2]$ , Earth-like  $[N_2 + O_2]$ , Martian and Venusian-type  $[CO_2]$ ) cases we assume the exoplanet radius and mass to be  $1 R_{\text{Earth}}$  and  $1 M_{\text{Earth}}$ , respectively. Numerical simulation of super-Earths will be performed in the upcoming studies.

#### 2.4. Event-integrated Spectra of Extreme SPEs

We assume that stellar accelerated protons are isotropically distributed in space as they precipitate into the atmospheres of the modeled planets and have two different energy spectra represented by the SPE spectra derived for the Carrington-class event in 1859 (Townsend et al. 2006) and the 43rd ground-level enhancement (GLE) in 1989 (Xapsos et al. 2000), respectively.

The Carrington-class event is considered to be the largest eruptive event recorded in modern human history. However, according to Smart et al. (2006), proton energy spectra associated with the Carrington-class event were rather soft in

comparison with other solar flares that produce GLEs. Thus, the radiation dose at the ground level during the event is expected to be not significantly high, because only a small fraction of the high-energy protons (with energies over 3 GeV for an 1 bar atmosphere) and their secondary particles can penetrate into the deep atmosphere.

To estimate the maximum impact on the ground level, we therefore calculated the radiation dose during the solar flare in association with a harder proton spectrum, GLE43, which is one of the most significant GLEs that has occurred after satellite observations were started in the late 20th century. It should be noted that GLE43 was selected as a typical SPE associated with a hard proton spectrum to estimate the maximum impact of SPE exposure at deeper locations in the atmosphere, although its flare class was not extremely high (X13). GLE5 (1956 February 23) -type spectra were also considered as a relevant event for the survey.

Figure 3 illustrates event-integrated spectra of the GLE43 and the Carrington flare.

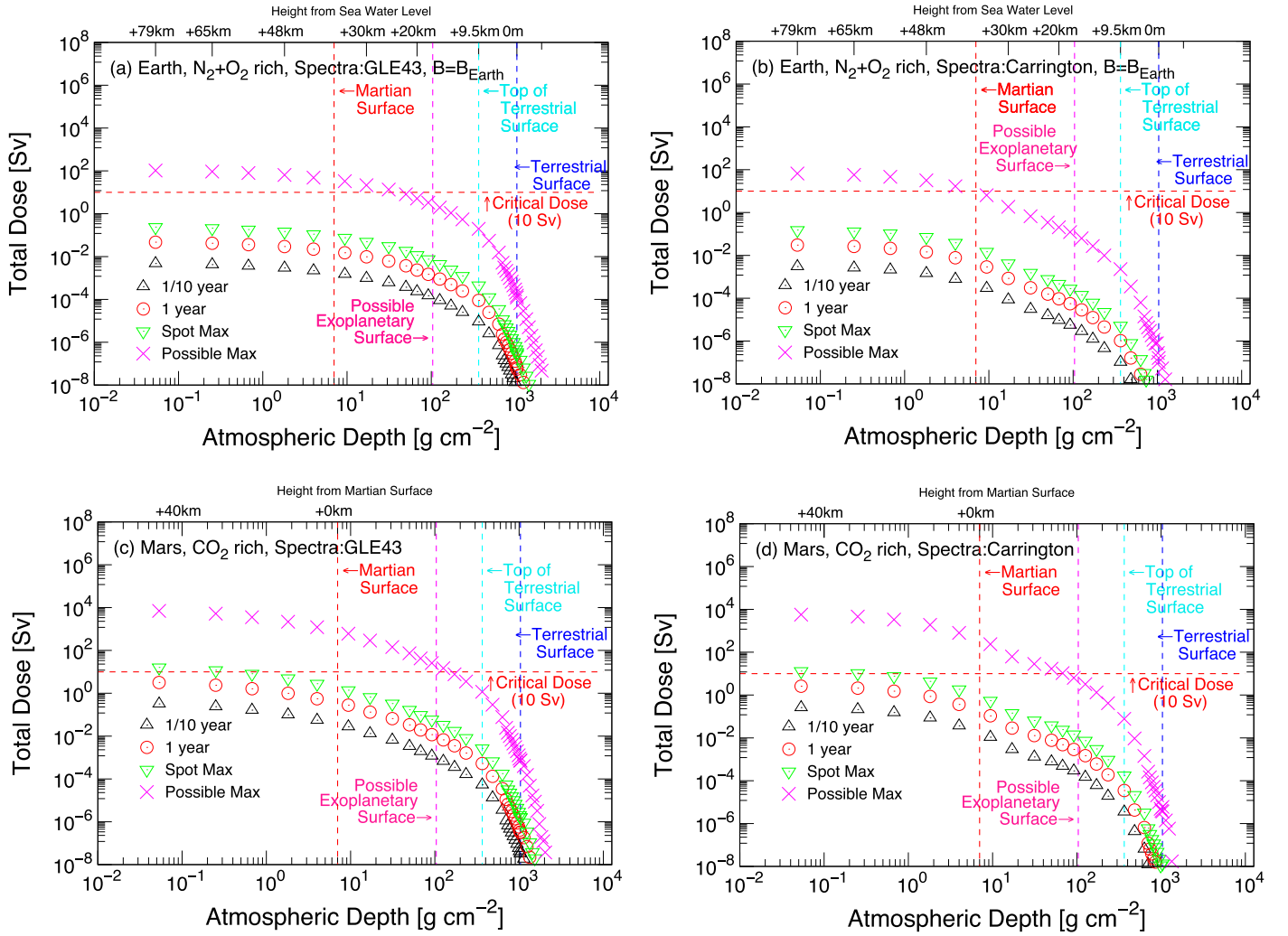


**Figure 6.** Vertical profile of radiation dose (in Sieverts) on Earth and Mars for possible flares on several different scales, caused by hard proton spectrum (imitating GLE43) (a and c) and soft spectrum (imitating Carrington) (b and d) penetrating  $N_2 + O_2$ -rich (terrestrial type) atmosphere for Earth (a and b) and  $CO_2$ -rich (Martian type) atmosphere for Mars (c and d) with flares every one-tenth of a year (36 days, black triangle), one year (red circle), spot maximum (green triangle), and possible maximum (red cross). Martian surface atmospheric pressure is equivalent to  $9 \text{ g cm}^{-2}$ ; terrestrial minimum atmospheric pressure, observed at the summit of the Himalayas, is equivalent to  $365 \text{ g cm}^{-2}$ ; (Earth's) ground-level atmospheric pressure is equivalent to  $1037 \text{ g cm}^{-2}$ ; possible exoplanetary surface is one-tenth of the terrestrial surface, equivalent to  $103.7 \text{ g cm}^{-2}$ .

### 2.5. The Influence of the Planetary Magnetic Field

We have simulated four scenarios of exoplanetary dipole magnetic moments: (1)  $B = 0$  (unmagnetized planet), (2)  $0.1 \times B_{\text{Earth}}$ , (3)  $1 \times B_{\text{Earth}}$  (Earth-like magnetic moment), and (4)  $10 \times B_{\text{Earth}}$ . The impact of the planetary magnetic field on the surface dose was modeled via the magnetospheric filter functions for the above four different magnetic moments, 0, 0.1, 1, and  $10 B_{\text{Earth}}$ , evaluated by Griebmeier et al. (2015).

The fluence of protons, neutrons, positive and negative muons, electrons, positrons, and photons was scored as a function of the atmospheric depth. They were then converted to the absorbed dose in grays and the effective dose in Sieverts (Sv) using the stopping power and the fluence to the dose conversion coefficients for the isotropic irradiation (International Commission on Radiological Protection, 2010), respectively. It should be mentioned that the effective dose is defined only for the purpose of radiological protection. However, we evaluated it for discussing the possible exposure effects on human-like life-forms because there is no alternative quantity that can be used for this discussion. More detailed descriptions

of the simulation procedures as well as their verification results for the solar energetic particle and galactic cosmic-ray simulation in the terrestrial atmosphere were given in our previous papers (Sato 2015; Sato et al. 2018b).

The impacts of all components produced by cosmic-ray interactions with the different atmospheric types in different layers were also individually evaluated and finally integrated to produce a final ground-level dose value for each simulated scenario. By examining all these different parameters together (atmospheric composition, geomagnetic field strength, and simulated cosmic-ray interactions), we have evaluated the atmospheric barrier needed for life on each of the target planets to survive a stellar flare event. This approach assumes that the potential life is as similarly radiation tolerant as that present on Earth.

### 2.6. The Maximum Stellar Flare Energy

Our goal is to study the effect of high ionizing particle fluxes caused by stellar activity on habitability of close-in Earth-sized and super-Earth exoplanets located within habitable zones.

**Table 2**  
Estimated Dose under Projected Flare Event—Annual Maximum Flare

Exoplanet Name	TOA <sup>a</sup> (Gy)	TOA <sup>b</sup> (Sv)	MS <sup>c</sup> (Gy)	MS <sup>d</sup> (Sv)	TM <sup>e</sup> (Gy)	TM <sup>f</sup> (Sv)	GL <sup>g</sup> (Gy)	GL <sup>h</sup> (Sv)
GJ 699 b	8.72E+01	3.95E+00	5.20E−01	3.46E−01	5.82E−05	5.91E−04	2.31E−08	2.59E−07
Kepler-283 c	9.64E+02	4.36E+01	5.75E+00	3.83E+00	6.44E−04	6.54E−03	2.56E−07	2.86E−06
Kepler-1634 b	3.84E+02	1.74E+01	2.29E+00	1.53E+00	2.56E−04	2.61E−03	1.02E−07	1.14E−06
Proxima Centauri b	9.37E+04	4.24E+03	5.60E+02	3.72E+02	6.26E−02	6.36E−01	2.49E−05	2.79E−04
Ross 128 b	4.36E+03	1.97E+02	2.60E+01	1.73E+01	2.91E−03	2.96E−02	1.16E−06	1.30E−05
TRAPPIST-1 b	4.97E+05	2.25E+04	2.97E+03	1.97E+03	3.32E−01	3.37E+00	1.32E−04	1.48E−03
TRAPPIST-1 c	2.65E+05	1.20E+04	1.58E+03	1.05E+03	1.77E−01	1.80E+00	7.04E−05	7.88E−04
TRAPPIST-1 d	1.33E+05	6.04E+03	7.97E+02	5.30E+02	8.91E−02	9.06E−01	3.54E−05	3.97E−04
TRAPPIST-1 e	7.73E+04	3.50E+03	4.61E+02	3.07E+02	5.16E−02	5.25E−01	2.05E−05	2.30E−04
TRAPPIST-1 f	4.46E+04	2.02E+03	2.66E+02	1.77E+02	2.98E−02	3.02E−01	1.18E−05	1.32E−04
TRAPPIST-1 g	3.02E+04	1.37E+03	1.80E+02	1.20E+02	2.01E−02	2.05E−01	8.00E−06	8.96E−05
TRAPPIST-1 h	1.55E+04	7.00E+02	9.22E+01	6.14E+01	1.03E−02	1.05E−01	4.10E−06	4.59E−05
Sol d (Earth)	1.64E+02	7.40E+00	9.76E−01	6.50E−01	1.09E−04	1.11E−03	4.34E−08	4.86E−07
Sol e (Mars)	7.05E+01	3.19E+00	4.21E−01	2.80E−01	4.71E−05	4.78E−04	1.87E−08	2.09E−07

**Notes.** TOA  $\approx 0 \text{ g cm}^{-2}$ . MS = Martian surface atmospheric pressure ( $9 \text{ g cm}^{-2}$ ); TM = terrestrial minimum atmospheric pressure ( $365 \text{ g cm}^{-2}$ ); GL = (Earth's) ground-level atmospheric pressure ( $1037 \text{ g cm}^{-2}$ ).

<sup>a</sup> Estimated dose (Gy) by annual maximum flare at TOA.

<sup>b</sup> Estimated dose (Sv) by annual maximum flare at TOA.

<sup>c</sup> Estimated dose (Gy) by annual maximum flare at MS.

<sup>d</sup> Estimated dose (Sv) by annual maximum flare at MS.

<sup>e</sup> Estimated dose (Gy) by annual maximum flare at TM.

<sup>f</sup> Estimated dose (Sv) by annual maximum flare at TM.

<sup>g</sup> Estimated dose (Gy) by annual maximum flare at GL.

<sup>h</sup> Estimated dose (Sv) by annual maximum flare at GL.

**Table 3**  
Estimated Dose under Projected Flare Event—Spot Maximum Flare

Exoplanet Name	TOA <sup>a</sup> (Gy)	TOA <sup>b</sup> (Sv)	MS <sup>c</sup> (Gy)	MS <sup>d</sup> (Sv)	TM <sup>e</sup> (Gy)	TM <sup>f</sup> (Sv)	GL <sup>g</sup> (Gy)	GL <sup>h</sup> (Sv)
GJ 699 b	1.60E+02	7.25E+00	9.56E−01	6.37E−01	1.07E−04	1.09E−03	4.25E−08	4.76E−07
Kepler-283 c	4.16E+03	1.89E+02	2.49E+01	1.65E+01	2.78E−03	2.83E−02	1.11E−06	1.24E−05
Kepler-1634 b	2.74E+03	1.24E+02	1.64E+01	1.09E+01	1.83E−03	1.86E−02	7.27E−07	8.14E−06
Proxima Centauri b	5.36E+05	2.43E+04	3.20E+03	2.13E+03	3.58E−01	3.64E+00	1.42E−04	1.59E−03
Ross 128 b	7.13E+03	3.23E+02	4.26E+01	2.83E+01	4.77E−03	4.84E−02	1.89E−06	2.12E−05
TRAPPIST-1 b	1.67E+06	7.58E+04	9.99E+03	6.65E+03	1.12E+00	1.14E+01	4.44E−04	4.97E−03
TRAPPIST-1 c	8.93E+05	4.04E+04	5.33E+03	3.55E+03	5.96E−01	6.06E+00	2.37E−04	2.65E−03
TRAPPIST-1 d	4.49E+05	2.03E+04	2.68E+03	1.79E+03	3.00E−01	3.05E+00	1.19E−04	1.34E−03
TRAPPIST-1 e	2.60E+05	1.18E+04	1.55E+03	1.03E+03	1.74E−01	1.77E+00	6.91E−05	7.74E−04
TRAPPIST-1 f	1.50E+05	6.79E+03	8.96E+02	5.96E+02	1.00E−01	1.02E+00	3.98E−05	4.46E−04
TRAPPIST-1 g	1.02E+05	4.60E+03	6.06E+02	4.04E+02	6.78E−02	6.89E−01	2.69E−05	3.02E−04
TRAPPIST-1 h	5.20E+04	2.36E+03	3.11E+02	2.07E+02	3.48E−02	3.53E−01	1.38E−05	1.55E−04
Sol d (Earth)	8.27E+02	3.74E+01	4.93E+00	3.29E+00	5.52E−04	5.61E−03	2.19E−07	2.46E−06
Sol e (Mars)	3.56E+02	1.61E+01	2.13E+00	1.42E+00	2.38E−04	2.42E−03	9.45E−08	1.06E−06

**Notes.** TOA  $\approx 0 \text{ g cm}^{-2}$ . MS = Martian surface atmospheric pressure ( $9 \text{ g cm}^{-2}$ ); TM = terrestrial minimum atmospheric pressure ( $365 \text{ g cm}^{-2}$ ); GL = (Earth's) ground-level atmospheric pressure ( $1037 \text{ g cm}^{-2}$ ).

<sup>a</sup> Estimated dose (Gy) by spot maximum flare at TOA.

<sup>b</sup> Estimated dose (Sv) by spot maximum flare at TOA.

<sup>c</sup> Estimated dose (Gy) by spot maximum flare at MS.

<sup>d</sup> Estimated dose (Sv) by spot maximum flare at MS.

<sup>e</sup> Estimated dose (Gy) by spot maximum flare at TM.

<sup>f</sup> Estimated dose (Sv) by spot maximum flare at TM.

<sup>g</sup> Estimated dose (Gy) by spot maximum flare at GL.

<sup>h</sup> Estimated dose (Sv) by spot maximum flare at GL.

CHZs around low-luminosity M dwarfs are located within 0.05 au, which suggests that many of them orbit their host stars within sub-Alfvénic distance and are subject to direct irradiation via high particle fluxes. To study the resulting surface dose we selected four exoplanets around active

M dwarfs, one exoplanet around K dwarfs with detected superflare, and one exoplanet around a G dwarf with higher stellar activity than our Sun. We selected the target stars for this survey according to the following procedure: (1) Select host star with exoplanet in habitable zone with direct superflare

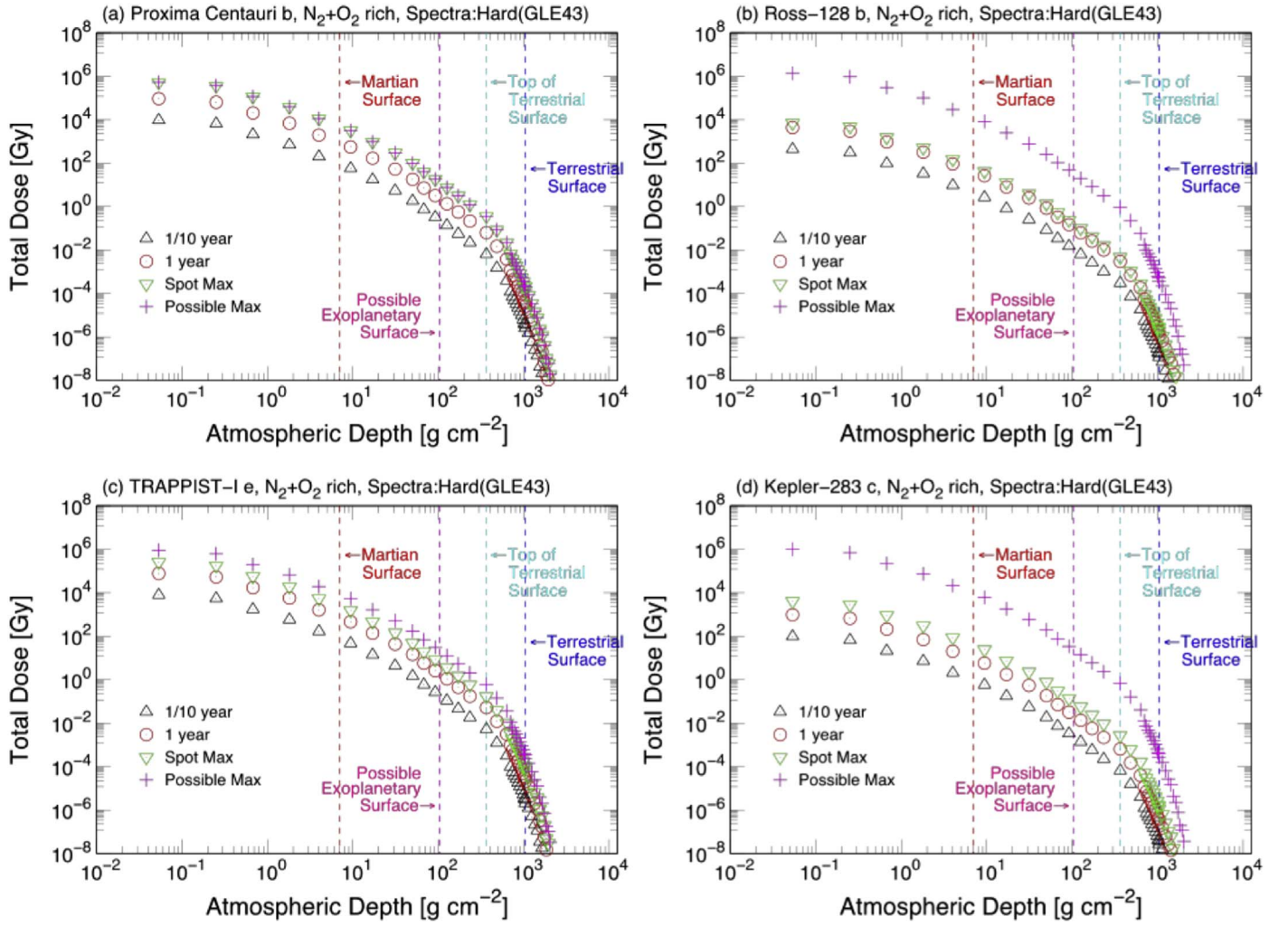


**Figure 7.** Vertical profile of radiation dose (in grays) on Proxima Centauri b, Ross-128 b, TRAPPIST-1e, and Kepler-283 c for possible flares on several different scales, caused by hard proton spectrum (imitating GLE43), penetrating  $N_2 + O_2$ -rich (terrestrial type) atmosphere for Earth with flares every one-tenth of a year (36 days, black triangle), one year (red circle), spot maximum (green triangle), and possible maximum (pink cross). Martian surface atmospheric pressure is equivalent to  $9 \text{ g cm}^{-2}$ ; terrestrial minimum atmospheric pressure, observed at the summit of the Himalayas, is equivalent to  $365 \text{ g cm}^{-2}$ ; (Earth's) ground-level atmospheric pressure is equivalent to  $1037 \text{ g cm}^{-2}$ ; possible exoplanetary surface is one-tenth of the terrestrial surface, equivalent to  $103.7 \text{ g cm}^{-2}$ .

observation through *Kepler* observation (Kepler-283). (2) Select *Kepler* stars whose flare frequency and magnitude can be estimated from their activities (Kepler-1634). (3) Select well-documented host star for well-documented exoplanets (GJ699 (Barnard's Star), Proxima Centauri, Ross-128, TRAPPIST-1). Stellar activities for all stars are estimated using their light curves.

Shibata et al. (2013) estimated the maximum value (upper limit) of flare energy, which is determined by the star spot area and magnetic field strength. We used this methodology to calculate the theoretical maximum flare energy for six host stars using their star spot areas:  $1.15 \times 10^{32}$  erg for GJ 699 (Barnard's star),  $2.13 \times 10^{33}$  erg for Kepler-283,  $1.18 \times 10^{34}$  erg for Kepler-1634,  $5.55 \times 10^{33}$  erg for Proxima Centauri,  $7.72 \times 10^{31}$  erg for Ross 128, and  $9.09 \times 10^{32}$  erg for TRAPPIST-1.

With this method, the current observed star spot area in each star restricts the maximum flare energy. However, it is unclear whether the observed period represents the maximum or minimum activity of the star. Accordingly, we also evaluated the potential maximum energy of the stellar flare by the following method.

For those stars whose stellar temperature is above 4000 K, we estimated maximum flare energy based on the relationship between *Kepler* stars by comparing their maximum observed energy and stellar temperature as well as their associated radii (H. Maehara 2019, private communication).

For those stars whose stellar temperature is below 4000 K, we assumed, in the extreme situation, that 20% of the stellar surface is covered by a star spot. Considering the extreme condition, we calculated the maximum energy using Shibata et al. (2013).

By introducing flare energy as the input for considerable maximum energy of the superflares for their planetary systems, we may theoretically calculate the possible maximum dose for their host planets.

### 3. Results

#### 3.1. Validation for Normal Dose

Figure 4 shows the vertical profile of radiation dose on Earth and Mars caused by SPEs with the hard proton spectrum (imitating GLE43) (a and b), and soft spectrum (imitating



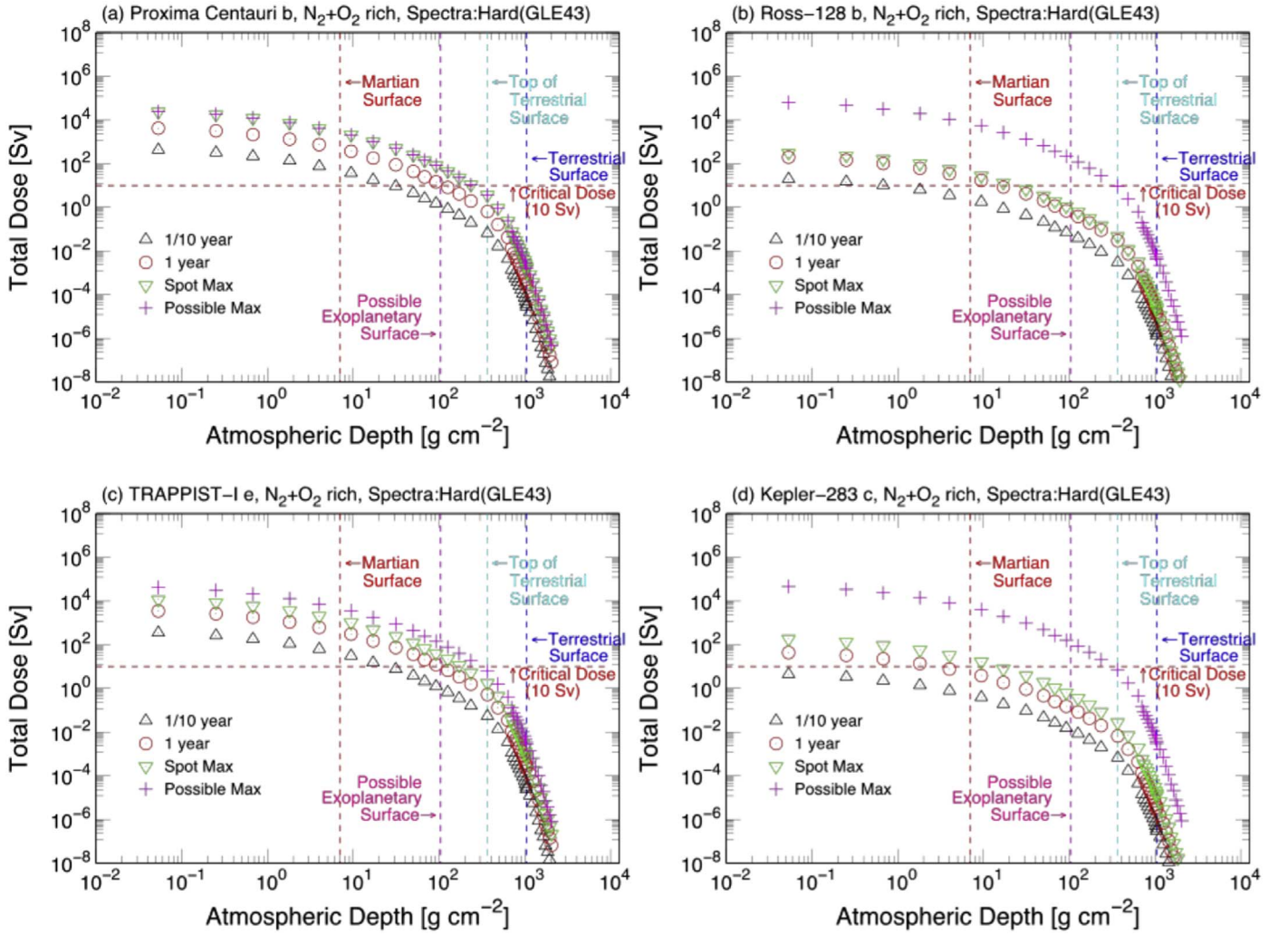


**Figure 8.** Vertical profile of radiation dose (in Sieverts) on Proxima Centauri b, Ross-128 b TRAPPIST-Ie, and Kepler-283 c for possible flares on several different scales, caused by hard proton spectrum (imitating GLE43) (a and c) and soft spectrum (Townsend Carrington) (b and d) penetrating  $N_2 + O_2$ -rich (terrestrial type) atmosphere for Earth with flares every one-tenth of a year (36 days, black triangle), one year (red circle), spot maximum (green triangle), and possible maximum (rose cross). Martian surface atmospheric pressure is equivalent to  $9\ g\ cm^{-2}$ ; terrestrial minimum atmospheric pressure, observed at the summit of the Himalayas, is equivalent to  $365\ g\ cm^{-2}$ ; (Earth's) ground-level atmospheric pressure is equivalent to  $1037\ g\ cm^{-2}$ ; possible exoplanetary surface is one-tenth of the terrestrial surface, equivalent to  $103.7\ g\ cm^{-2}$ .

Carrington) (c and d), penetrating  $N_2 + O_2$ -rich (terrestrial-type) atmosphere Earth with  $10^{30}$  erg (black triangle),  $10^{32}$  erg (red circle),  $10^{34}$  erg (blue square), and  $10^{36}$  erg (red cross) in grays (a and c) and Sieverts (b and d). This figure shows that the radiation dose at the tropopause (around  $170\ g\ cm^{-2}$  atmospheric depth) becomes  $0.5\ mSv$ , which mostly agrees with the aerial observation, when the solar flare energy is scaled to  $E_0 = 10^{32}$ . Note that this normalization has been made for an idealized series of flares, considering the horizontal angle of the SPE injection as  $90^\circ$ ; in other words, the probability of reaching Earth is one in four.

Figures 5 and 6 show vertical profile of radiation dose in grays and Sieverts, respectively, on Earth and Mars for possible flares on several different scales, caused by hard proton spectrum (imitating GLE43) (a and c) and soft spectrum (imitating Carrington reproduced by Townsend et al. 2006) (b and d) penetrating  $N_2 + O_2$ -rich (terrestrial-type) atmosphere for Earth (a and b) and  $CO_2$ -rich (Martian type) atmosphere for Mars (c and d), with flares every one-tenth of a year (36 days, corresponding to  $7.2 \times 10^{31}$  erg), one year (corresponding to

$7.2 \times 10^{32}$  erg), spot maximum flare (corresponding to  $3.6 \times 10^{33}$  erg), and possible maximum flare (corresponding to  $1.6 \times 10^{36}$  erg). In these scenarios, the spot maximum flare is the maximum possible flare observed within decades in the target stellar system (in this case our solar system) estimated based on star spot area of the target star. According to the calculation shown in these figures, the SPEs under the above scenarios do not induce a critical dose at ground level when we have sufficient atmospheric depth such as Earth, even under the possible maximum flare ( $1.6 \times 10^{36}$  erg) scenario, whereas it becomes a nearly critical dose on the Martian surface with thinner atmospheric depth when the spot maximum flare ( $3.6 \times 10^{33}$  erg) event occurs.

### 3.2. Estimated Dose on Exoplanetary Surface under Different Flare Scenarios

The estimated doses under the annual maximum flare and under the spot maximum flare are shown in Tables 2 and 3, respectively. The estimated doses at the TOA on GJ 699 b, Proxima Centauri b,

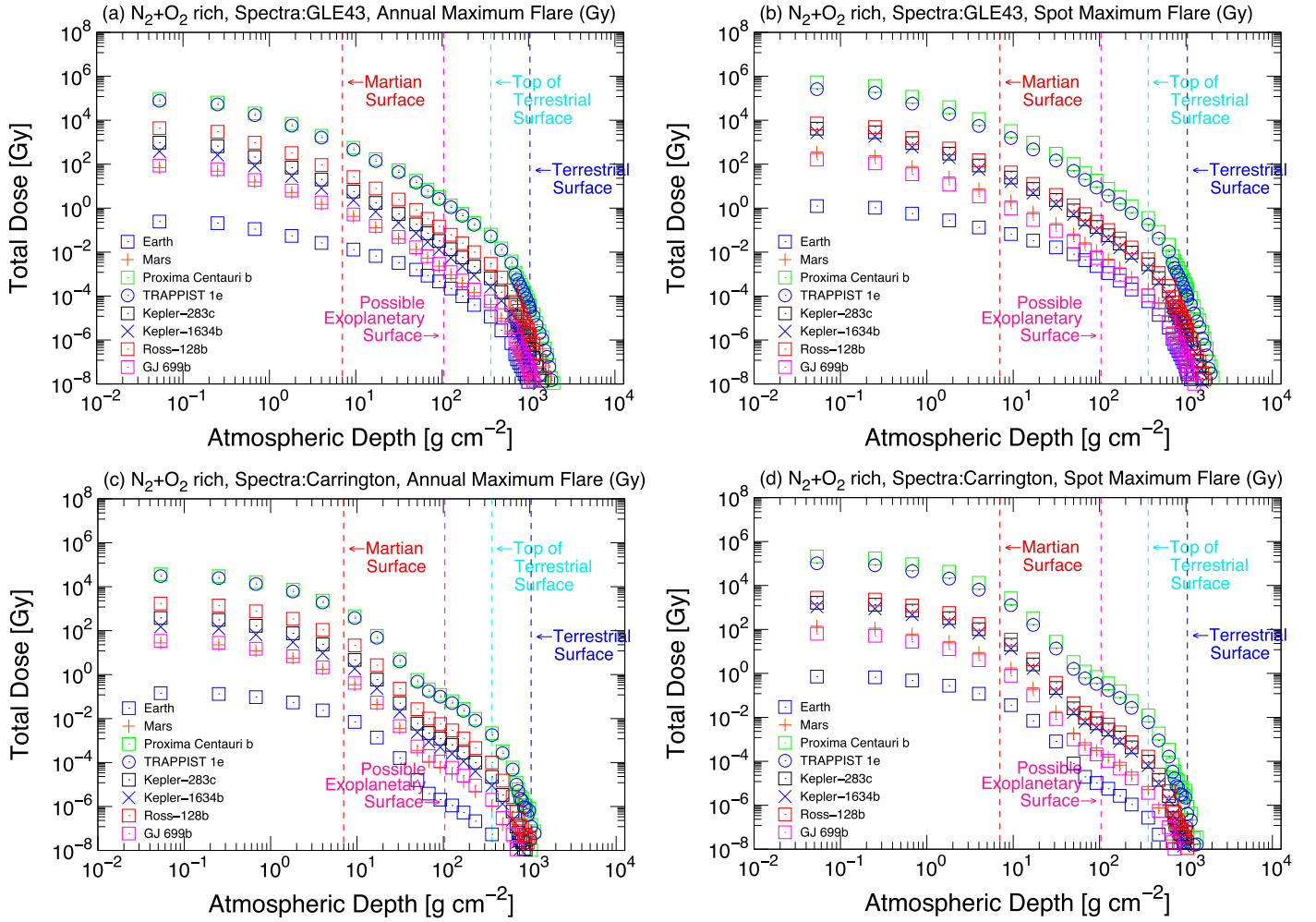


**Figure 9.** Vertical profile of radiation dose (in grays), caused by proton spectrum imitating GLE43 (a and b) and Carrington Flare (c and d) penetrating  $N_2 + O_2$ -rich (terrestrial type) atmosphere on Proxima Centauri b (green square), TRAPPIST-1 e (blue circle), Kepler-283 c (brown square), Kepler-1634 b (blue cross), Ross-128 b (red square), and GJ-699 b (pink square) in comparison with the Earth (blue square) and Mars (red plus) in logarithmic scale under annual maximum flare energy (a and c) and under spot maximum flare energy (b and d), in grays. Martian surface atmospheric pressure is equivalent to  $9 \text{ g cm}^{-2}$ ; terrestrial minimum atmospheric pressure, observed at the summit of the Himalayas, is equivalent to  $365 \text{ g cm}^{-2}$ ; (Earth's) ground-level atmospheric pressure is equivalent to  $1037 \text{ g cm}^{-2}$ ; possible exoplanetary surface is one-tenth of the terrestrial surface, equivalent to  $103.7 \text{ g cm}^{-2}$ .

Ross-128 b, and TRAPPIST-1 e under the spot maximum flare (Shibata et al. 2013) become  $1.60 \times 10^2 \text{ Gy}$  ( $7.25 \text{ Sv}$ ),  $5.36 \times 10^5 \text{ Gy}$  ( $2.43 \times 10^4 \text{ Sv}$ ),  $7.13 \times 10^3 \text{ Gy}$  ( $3.23 \times 10^2 \text{ Sv}$ ), and  $2.60 \times 10^5 \text{ Gy}$  ( $1.18 \times 10^4 \text{ Sv}$ ), respectively.

Figures 7 and 8 illustrate the vertical radiation dose in grays and Sieverts, respectively, for major documented planetary systems, including Proxima Centauri b, Ross-128 b, TRAPPIST-1 e, and Kepler-283 c (the only habitable planet in the *Kepler* field with observed flares) for possible flares on several different scales, caused by hard proton spectrum (imitating GLE43) penetrating  $N_2 + O_2$ -rich (terrestrial type) atmosphere for Earth with flares every one-tenth of a year (36 days), one year (annual), spot maximum, and possible maximum flare. In these scenarios, the spot maximum flare is the maximum possible flare to be observed within decades in the target stellar system. On these planets, the SPE does not reach critical levels with sufficient atmospheric depth (equal to that of the Earth) even for the possible maximum flare scenario, having  $1.42 \times 10^{-4} \text{ Gy}$  ( $1.6 \times 10^{-3} \text{ Sv}$ ) for Proxima Centauri b and  $3.70 \times 10^{-4} \text{ Gy}$  ( $4.14 \times 10^{-3} \text{ Sv}$ ) for Ross-128 b. Proxima Centauri b shows a smaller difference between the possible maximum flare dose and

spot maximum flare dose, whereas a larger difference can be found on Ross-128 b, showing that Ross-128b is relatively calm in the range of the same temperature class.

However, when considering the possible maximum flare, calculated assuming that the whole star is covered by the maximum percentage of star spot (20%, observed from Proxima Centauri's light-curve survey), the estimated radiation dose at the terrestrial lowest atmospheric thickness measured at the summit of Everest (at AD  $365 \text{ g cm}^{-2}$  set in this study) applied to Proxima Centauri b, Ross-128 b, TRAPPIST-1 e, and Kepler-283 c, reaches a fatal dose of  $0.36 \text{ Gy}$  ( $3.64 \text{ Sv}$ ),  $0.93 \text{ Gy}$  ( $9.45 \text{ Sv}$ ),  $3.03 \text{ Gy}$  ( $30.8 \text{ Sv}$ ), and  $0.68 \text{ Gy}$  ( $6.89 \text{ Sv}$ ), respectively.

We calculated the vertical profile of the radiation dose, caused by the proton spectrum similar to the one reconstructed for the GLE43 and Carrington-class events for each planet (GJ-699b, Kepler-283 c, Kepler-1634 b, Proxima Centauri b, Proxima Centauri b, Ross 128 b, TRAPPIST-1 e), with terrestrial-type atmospheric compositions under annual maximum flare and spot maximum flare events, by comparing that of Earth and Mars (see Figures 9 and 10).

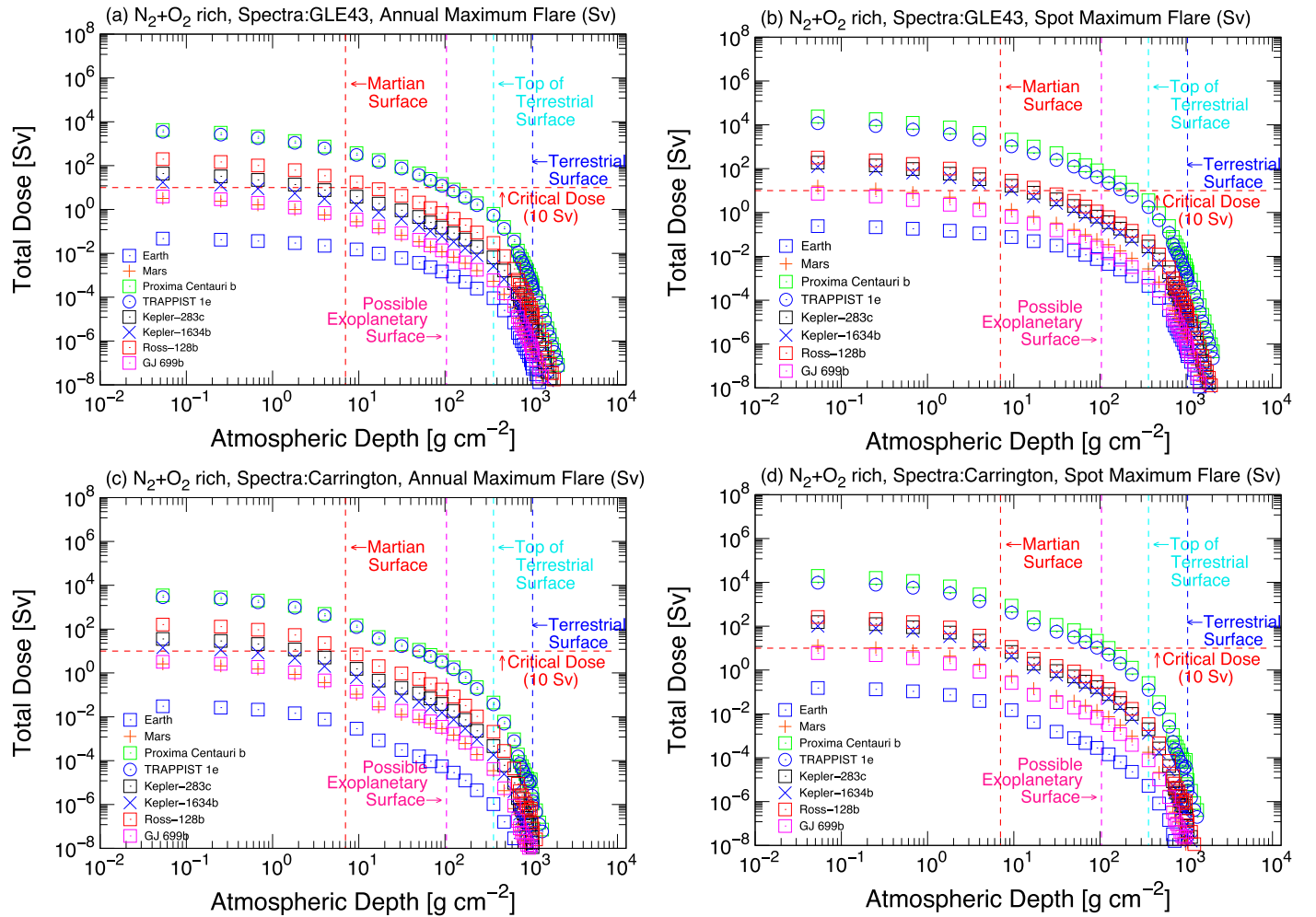


**Figure 10.** Vertical profile of radiation dose (in Sieverts), caused by proton spectrum imitating GLE43 (a and b) and Carrington flare (c and d) penetrating  $N_2 + O_2$ -rich (terrestrial type) atmosphere on Proxima Centauri b (green square), TRAPPIST-1 e (blue circle), Kepler-283 c (brown square), Kepler-1634 b (blue cross), Ross-128 b (red square), and GJ-699 b (pink square) in comparison with the Earth (blue square) and Mars (red plus) in logarithmic scale under annual maximum flare energy (a and c) and under spot maximum flare energy (b and d), in Sieverts. Martian surface atmospheric pressure is equivalent to  $9 \text{ g cm}^{-2}$ ; terrestrial minimum atmospheric pressure, observed at the summit of the Himalayas, is equivalent to  $365 \text{ g cm}^{-2}$ ; (Earth's) ground-level atmospheric pressure is equivalent to  $1037 \text{ g cm}^{-2}$ ; possible exoplanetary surface is one-tenth of the terrestrial surface, equivalent to  $103.7 \text{ g cm}^{-2}$ .

For the evaluation at different atmospheric depths we employed the following four typical atmospheric depth reference layers: TOA is equivalent to  $\approx 0 \text{ g cm}^{-2}$ ; Martian surface atmospheric pressure (MS) is equivalent to  $9 \text{ g cm}^{-2}$ ; terrestrial minimum atmospheric pressure, observed at the summit of the Himalayas, is equivalent to  $365 \text{ g cm}^{-2}$  in this study; and (Earth's) ground-level atmospheric pressure is equivalent to  $1037 \text{ g cm}^{-2}$ . Possible exoplanetary surface was estimated as one-tenth of the terrestrial surface, equivalent to  $103.7 \text{ g cm}^{-2}$ . Note that the value is not identical to the real observation data but to the nearest value employed in the Monte Carlo numerical simulation.

According to these calculations, we can specify the critical dose for each planet, which is presumed in this study to be  $10 \text{ Sv}$  per annual event (see Section A.1. of the Appendix). Using this threshold, we may determine the minimum requirement of the atmospheric depth for terrestrial-type life-form evolution. According to our analysis, the critical atmospheric depths required to secure terrestrial-type life-form evolution on the surface of each modeled exoplanet exposed by annual severe flare events are  $2.77 \text{ g cm}^{-2}$  for GJ 699 b

(Barnard's Star b) ( $0.267\%$  of terrestrial atmospheric depth),  $3.27 \times 10^2 \text{ g cm}^{-2}$  for Proxima Centauri b ( $31.6\%$  of terrestrial atmospheric depth),  $7.59 \times 10 \text{ g cm}^{-2}$  ( $7.31\%$ ) for Ross 128 b, and  $3.06 \times 10^2 \text{ g cm}^{-2}$  for TRAPPIST-1 e ( $29.5\%$ ) (Figures 9 and 10). We note that without sufficient atmospheric depth, the surface primitive life-forms on those planets suffer from severe radiation doses, even for relatively small-scale flares.

We also performed calculations of the radiation doses for  $CO_2$ -rich and  $H_2$ -rich atmospheres for each planet (see Figures 11–14). The difference between each atmospheric composition does not become significant especially when compared with the  $N_2 + O_2$ - and  $CO_2$ -rich types. However, it is evident that  $H_2$ -rich atmosphere dissipates higher energetic particles more significantly.

The presence of a geomagnetic dipole shield around a planet and its relative strength will influence its efficacy for reducing the irradiation effect of any solar flares on surface life-forms. First, we recalculated the surface dose (grays and Sieverts) assuming that all exoplanets (GJ-699 b, Kepler-283 c, Kepler-1634 b, Proxima Centauri b, Ross-128 b, TRAPPIST-1 e in comparison with Earth and Mars) have the same amount of



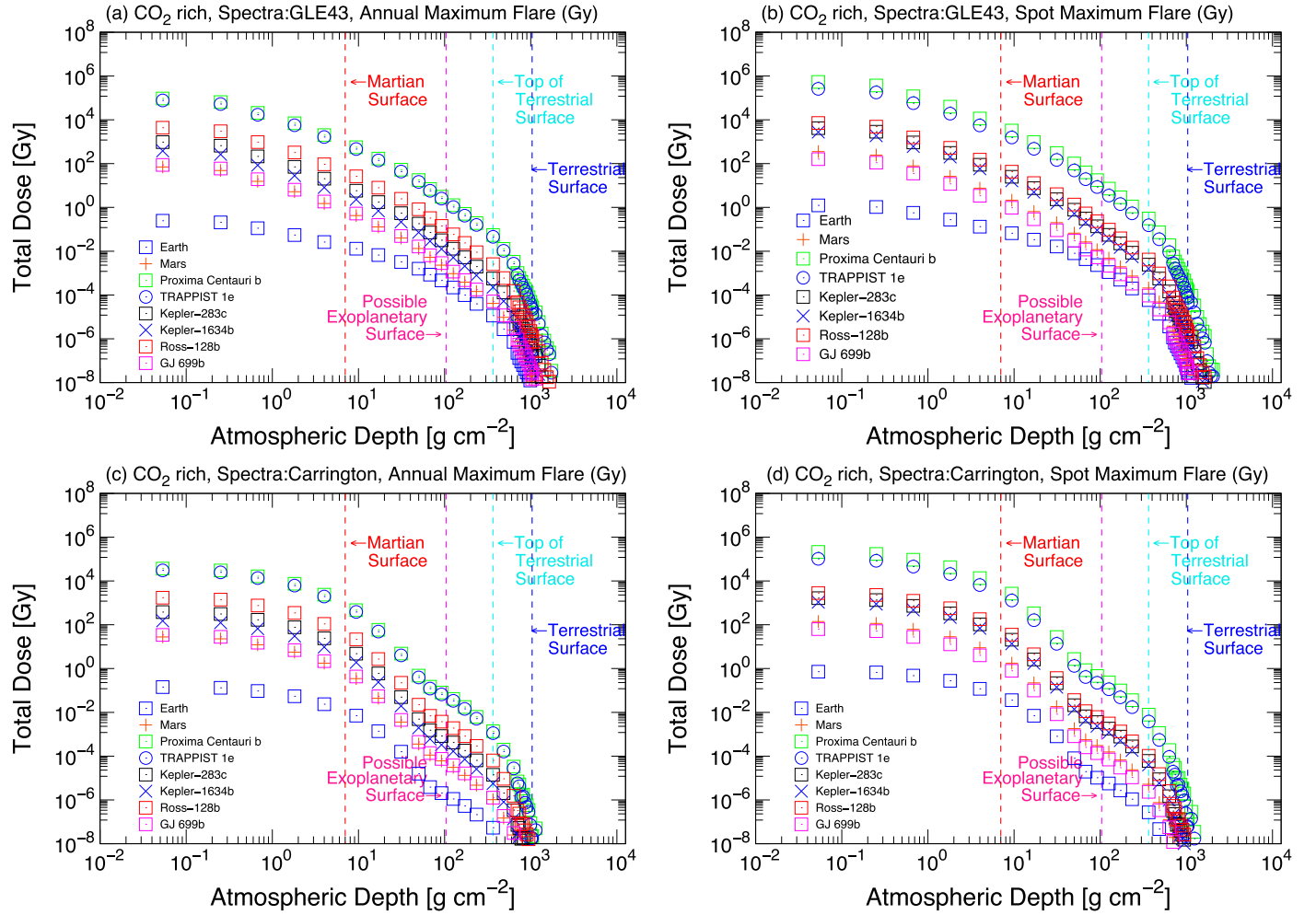


**Figure 11.** Vertical profile of radiation dose (in grays), caused by proton spectrum imitating GLE43 (a and b) and Carrington flare (c and d) penetrating CO<sub>2</sub>-rich (terrestrial type) atmosphere on Proxima Centauri b (green square), TRAPPIST-1 e (blue circle), Kepler-283 c (brown square), Kepler-1634 b (blue cross), Ross-128 b (red square), and GJ-699 b (pink square) in comparison with the Earth (blue square) and Mars (red plus) in logarithmic scale under annual maximum flare energy (a and c) and under spot maximum flare energy (b and d), in grays. Martian surface atmospheric pressure is equivalent to  $9 \text{ g cm}^{-2}$ ; terrestrial minimum atmospheric pressure, observed at the summit of the Himalayas, is equivalent to  $365 \text{ g cm}^{-2}$ ; (Earth's) ground-level atmospheric pressure is equivalent to  $1037 \text{ g cm}^{-2}$ ; possible exoplanetary surface is one-tenth of the terrestrial surface, equivalent to  $103.7 \text{ g cm}^{-2}$ .

magnetic shield as the Earth ( $B = B_{\text{Earth}}$ ) (see Figures 15 and 16). Then we evaluated the scenarios with the planetary dipole magnetic field (uniform over the whole planet surface) of (1) 0 (no magnetosphere), (2)  $0.1 \times B_{\text{Earth}}$ , (3)  $1 \times B_{\text{Earth}}$  (Earth level), and (4)  $10 \times B_{\text{Earth}}$  for four documented exoplanets (Proxima Centauri b, Ross-128b, and TRAPPIST-1 e, and Kepler-283 c) (see Figure 17).

### 3.3. Atmospheric Escape Induced by XUV Flux and Associated Possible Higher Radiation Dose

XUV radiation caused by stellar superflares does not significantly increase the annual planetary surface UV flux on the exoplanets modeled unless high stellar magnetically driven events (flares and CMEs) severely damage their atmospheric thickness and impact their chemistry. However, since stellar quiescent XUV radiation induces atmospheric escape from a terrestrial-type planet, a more critical situation may be predicted, that is, the atmospheric depth of those exoplanets can easily reach at least one-tenth of terrestrial atmospheric thickness. The atmospheric escape rate of  $\text{O}^+/\text{N}^+$  ions

from Proxima Centauri b, TRAPPIST-1 e, Ross-128b, and Kepler-283 c are, respectively, 76.2, 53.5, 7.92, and 6.82 times stronger than that of the Earth due to higher stellar XUV fluxes incident on the planetary atmospheres caused by closer proximity to their respective host stars according to the equation proposed by Airapetian et al. (2017a).

In such a scenario, the radiation dose at Proxima Centauri b and TRAPPIST-1 e reaches nearly fatal levels for complex life-forms even through the modest annual flares, reaching 1.32 Gy (8.09 Sv) and 1.09 Gy (6.68 Sv), respectively (see Figure 8).

## 4. Discussion and Future Work

### 4.1. Estimated Dose by Stellar Proton Event in Exoplanets

The stellar proton event impact onto different exoplanets has been evaluated assuming three major types of atmosphere ( $\text{N}_2 + \text{O}_2$ ,  $\text{CO}_2$ ,  $\text{H}_2$ ). In general,  $\text{H}_2$ -rich atmosphere, which may be present on either younger Earth-sized exoplanets or super-Earths with relatively larger masses, has a maximum absorption ratio compared with the other two atmospheres.



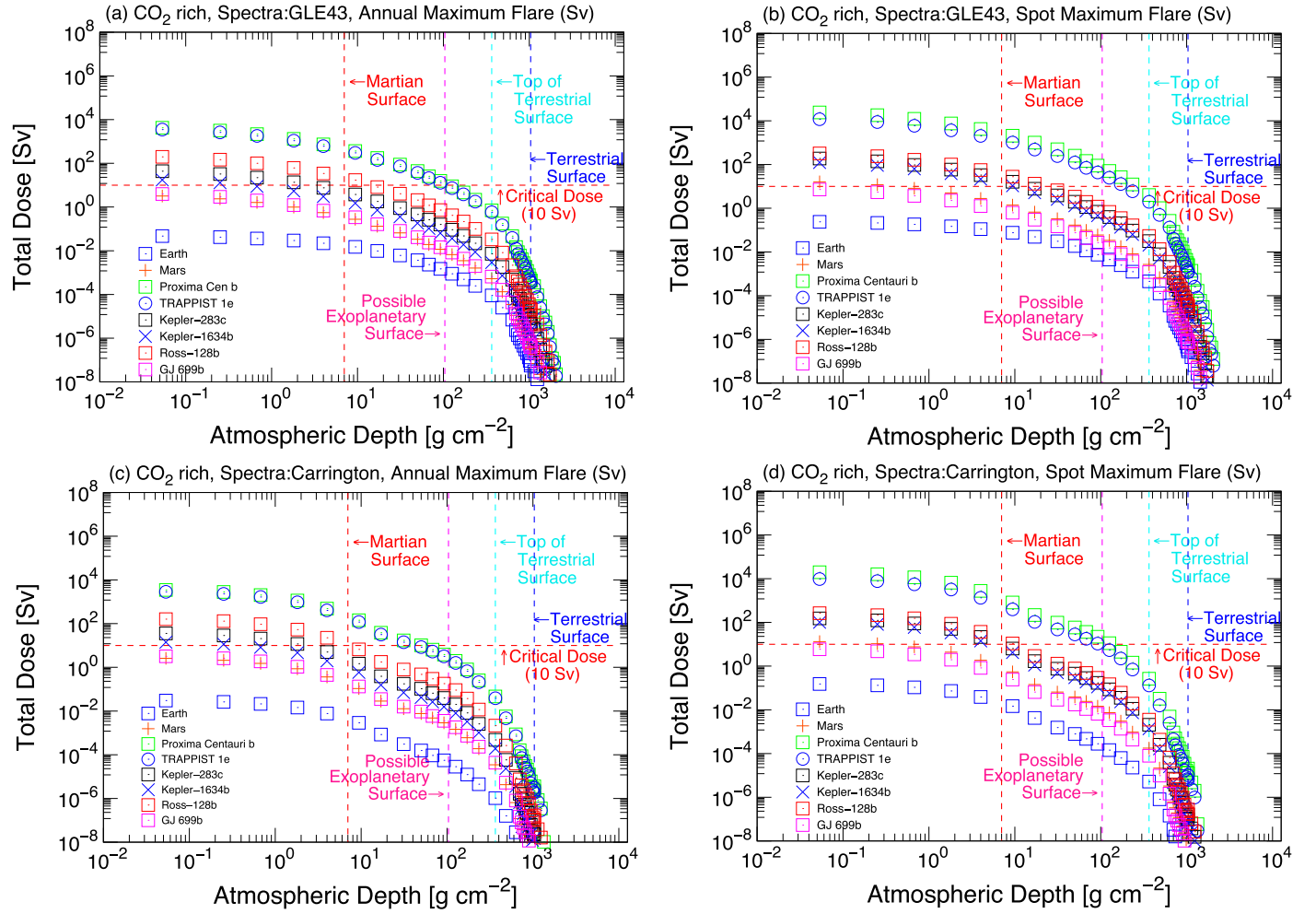


**Figure 12.** Vertical profile of radiation dose (in Sieverts), caused by proton spectrum imitating GLE43 (a and b) and Carrington flare (c and d) penetrating CO<sub>2</sub>-rich (terrestrial type) atmosphere on Proxima Centauri b (green square), TRAPPIST-1 e (blue circle), Kepler-283 c (brown square), Kepler-1634 b (blue cross), Ross-128 b (red square), and GJ-699 b (pink square) in comparison with the Earth (blue square) and Mars (red plus) in logarithmic scale under annual maximum flare energy (a and c) and under spot maximum flare energy (b and d), in Sieverts. Martian surface atmospheric pressure is equivalent to  $9 \text{ g cm}^{-2}$ ; terrestrial minimum atmospheric pressure, observed at the summit of the Himalayas, is equivalent to  $365 \text{ g cm}^{-2}$ ; (Earth's) ground-level atmospheric pressure is equivalent to  $1037 \text{ g cm}^{-2}$ ; possible exoplanetary surface is one-tenth of the terrestrial surface, equivalent to  $103.7 \text{ g cm}^{-2}$ .

This might be because of the lower molecular weight of hydrogen, which enables larger molecular numbers under the same atmospheric pressure. Under the other two major types of atmosphere ( $\text{N}_2 + \text{O}_2$ ,  $\text{CO}_2$ ), there are still significant reduction effects when atmospheric pressure is sufficient as that of the Earth. For TRAPPIST-1 e and Proxima Centauri b, even for annual maximum flare events, the dose becomes relatively large but not at the level that may affect complex life-forms. However, with reduced atmospheric pressure to the level at the top of the terrestrial surface ( $352 \text{ g cm}^{-2}$ ), observed at the summit of the Himalayas, the dose becomes significantly high. The dose with higher atmospheric depth than the Martian surface, especially in units of Sieverts, has been evaluated to be higher than in previous papers calculated by different approaches with hypothetical stellar flare magnitude (Atri 2017). This may be induced by the difference in definitions of the effective doses, as well as precise numerical evaluation using PHITS (Sato et al. 2018b). This relatively higher dose in Sieverts compared with the unit in grays, calculated at the higher atmospheric depth than Martian

surface, is mainly induced by the neutron particle, generated as a secondary cosmic-ray when SEP reaches the atmosphere, as shown in Figures 18 and 19.

Our conclusion is that, with relevant thickness of atmospheric depth for each type of atmosphere, there will be no significant damage to surface life-forms, except for some critical planets located very close to their stars.

Projected stellar proton events with harder spectra using GLE43 have a deeper penetration of intensive protons toward the terrestrial atmospheric depth, whereas projected stellar proton events with softer spectra using the Carrington flare have a sudden reduction of the dose at the mid altitude of the atmosphere (atmospheric depth between  $10^1$  and  $10^2 \text{ g cm}^{-2}$ ).

By taking a look at Figure 16, most of the critical dose only applies for Proxima Centauri b and TRAPPIST-1 e when the atmospheric depth was lower than that of Martian surface when all exoplanets have the same amount of magnetic shield as Earth ( $B = B_{\text{Earth}}$ ), except for the scenario with spot maximum flare with proton spectrum imitating GLE43 (b). Each value of the magnetic field may result in a significant dose reduction at

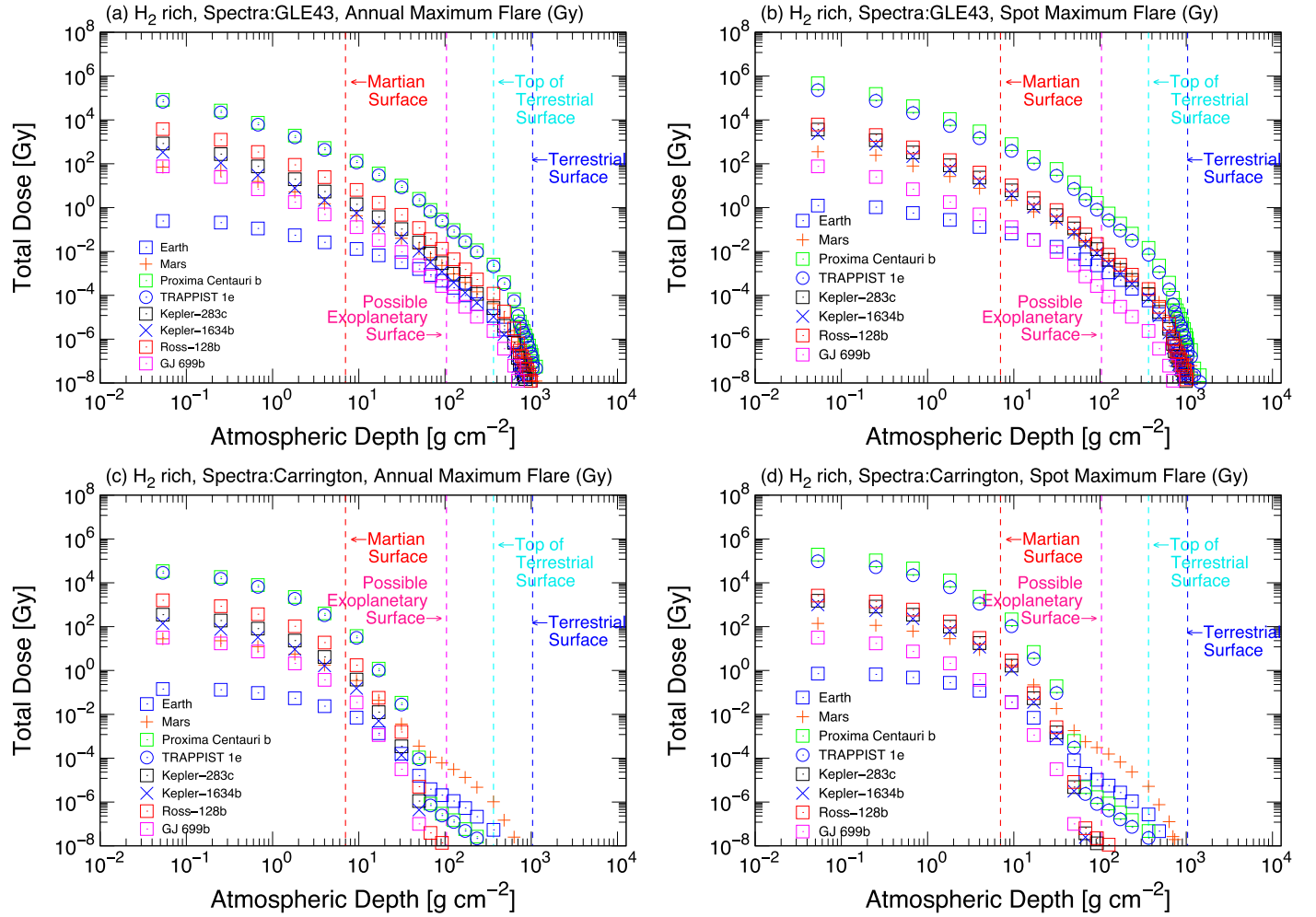


**Figure 13.** Vertical profile of radiation dose (in Sieverts), caused by proton spectrum imitating GLE43 (a and b) and Carrington flare (c and d) penetrating  $\text{H}_2$ -rich (terrestrial type) atmosphere on Proxima Centauri b (green square), TRAPPIST-1 e (blue circle), Kepler-283 c (brown square), Kepler-1634 b (blue cross), Ross-128 b (red square), and GJ-699 b (pink square) in comparison with the Earth (blue square) and Mars (red plus) in logarithmic scale under annual maximum flare energy (a and c) and under spot maximum flare energy (b and d), in grays. Martian surface atmospheric pressure is equivalent to  $9 \text{ g cm}^{-2}$ ; terrestrial minimum atmospheric pressure, observed at the summit of the Himalayas, is equivalent to  $365 \text{ g cm}^{-2}$ ; (Earth's) ground-level atmospheric pressure is equivalent to  $1037 \text{ g cm}^{-2}$ ; possible exoplanetary surface is one-tenth of the terrestrial surface, equivalent to  $103.7 \text{ g cm}^{-2}$ .

the TOA, from (1)  $9.37 \times 10^4 \text{ Gy}$  ( $4.24 \times 10^3 \text{ Sv}$ ) with no magnetosphere to (3)  $1.40 \times 10^2 \text{ Gy}$  ( $2.7 \times 10^1 \text{ Sv}$ ) with Earth-level magnetosphere ( $1 \times B_{\text{Earth}}$ ) almost 1/700 of the dose in grays (1/160 in Sv) that would be received with no protective magnetic field. Also at the ground level, the dose was reduced from (1)  $2.49 \times 10^{-5} \text{ Gy}$  ( $2.79 \times 10^{-5} \text{ Sv}$ ) with no magnetosphere, to (3)  $3.23 \times 10^{-6} \text{ Gy}$  ( $3.19 \times 10^{-5} \text{ Sv}$ ) with Earth-level magnetosphere ( $1 \times B_{\text{Earth}}$ ) on Proxima Centauri b, almost one-tenth of the dose that would be received with no protective magnetic field. We may consider that, with the presence of magnetic shields, those listed planets all become habitable at least when the minimum amount of atmospheric depth is present.

#### 4.2. Impact of XUV Radiation

We also evaluated XUV flux values from stellar flares as follows (see Section A.4. in the Appendix). Here we assume that the UV energy portion is up to 10% of the total flare energy and estimate XUV dose by annual maximum flare. As a result,

annual XUV dose values due to stellar flares at the TOA of the target exoplanets are  $10^5 \sim 10^6 \text{ J m}^{-2}$  (see Table 2). They are all smaller than 0.001% of the terrestrial annual UV dose at the TOA ( $\sim 4.3 \times 10^9 \text{ J m}^{-2}$ ).

In addition to estimating the flare XUV values, we also roughly evaluate the quiescent component of XUV fluxes from stellar temperature (spectral class) and spot size (see Section A.4. of the Appendix). As a result, the annual total flux of the whole XUV and UV wavelength range ( $10\text{--}4000 \text{ \AA}$ ) at the TOA of all our target exoplanets is smaller than the annual total of the Earth. For example, in the most severe case, Kepler-1634b shows 56% of the Earth values. The impulsive UV doses from annual maximum flares are not significant when compared with the annual dose from steady components. In contrast, the XUV ( $1\text{--}1200 \text{ \AA}$ ) fluxes at the TOA of the target exoplanets have much higher values compared with those at Earth. For example, Proxima Centauri experiences  $\sim 76$  times larger annual XUV flux at its TOA compared with Earth's value, while TRAPPIST-1 e has  $\sim 65$  times larger flux values. This is because the XUV contribution in the overall UV

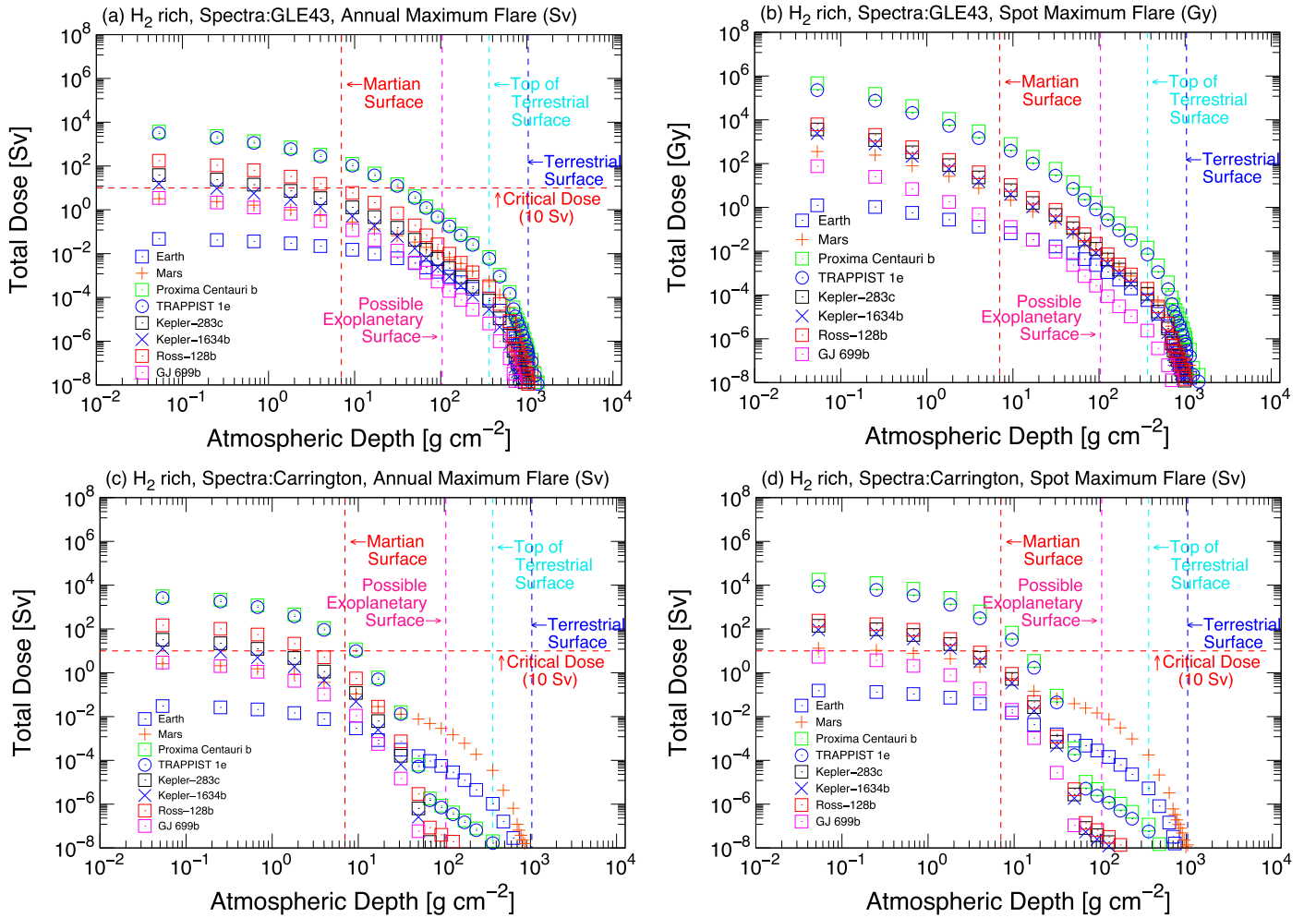


**Figure 14.** Vertical profile of radiation dose (in Sieverts), caused by proton spectrum imitating GLE43 (a and b) and Carrington flare (c and d) penetrating H<sub>2</sub>-rich (terrestrial type) atmosphere on Proxima Centauri b (green square), TRAPPIST-1 e (blue circle), Kepler-283 c (brown square), Kepler-1634 b (blue cross), Ross-128 b (red square), and GJ-699 b (pink square) in comparison with the Earth (blue square) and Mars (red plus) in logarithmic scale under annual maximum flare energy (a and c) and under spot maximum flare energy (b and d), in Sieverts. Martian surface atmospheric pressure is equivalent to  $9 \text{ g cm}^{-2}$ ; terrestrial minimum atmospheric pressure, observed at the summit of the Himalayas, is equivalent to  $365 \text{ g cm}^{-2}$ ; (Earth's) ground-level atmospheric pressure is equivalent to  $1037 \text{ g cm}^{-2}$ ; possible exoplanetary surface is one-tenth of terrestrial surface, equivalent to  $103.7 \text{ g cm}^{-2}$ .

emission from cool M dwarfs is larger than that for the Sun (Ribas et al. 2017).

#### 4.3. Estimation of Atmospheric Escape Rate due to Photoionization

Since coronal XUV radiation induces atmospheric escape via photoionization, we can estimate the atmospheric escape rate on Proxima Centauri b, TRAPPIST-1 e, Ross-128b, and Kepler-283 c using the proposed XUV flux escape rate scaling by Airapetian et al. (2017a). In order to estimate these values, we needed to obtain or synthesize the possible XUV flux for those hoststars. In this study, we calculated all XUV fluxes according to the method illustrated in the Appendix. After obtaining the XUV fluxes, we compared them with the atmospheric escape rate from the Earth. The atmospheric escape rates via quiescent XUV emission from Proxima Centauri b, TRAPPIST-1 e, Ross-128b, and Kepler-283 c are, respectively, 76.2, 53.5, 7.92, and 6.82 times stronger than that of the Earth due to the higher XUV fluxes incident on close-in exoplanetary atmospheres. If not enough outgassing

for these planets is expected, the assumed atmospheric depths especially for Proxima Centauri b and TRAPPIST-1 e may reach  $\leq 1/10$  of the atmospheric pressure on Earth. In such a scenario, the radiation dose on Proxima Centauri b and TRAPPIST-1 e reach nearly fatal levels even through annual flares, reaching 1.32 Gy (8.09 Sv) and 1.09 Gy (6.68 Sv), respectively (see Figures 7 and 8).

#### 4.4. Summary of XUV Studies

The following items are not well characterized in the presented models: (1) the MUSCLES survey provides stellar spectra ranging from XUV to IR based on observed (*Chandra* and *XMM* and *HST*) and empirical estimates. However, the MUSCLES study includes stars earlier than M4 dwarfs ( $T_{\text{eff}} > 3000 \text{ K}$ ), and thus there are no relevant data for cooler stars, such as TRAPPIST-1, whose  $T_{\text{eff}}$  is almost 2500 K. Our models based on these assumptions should be updated with new observations to be performed in the near future (Airapetian et al. 2019). (2) The correlation between XUV fluxes and star spot sizes, assumed from previous solar

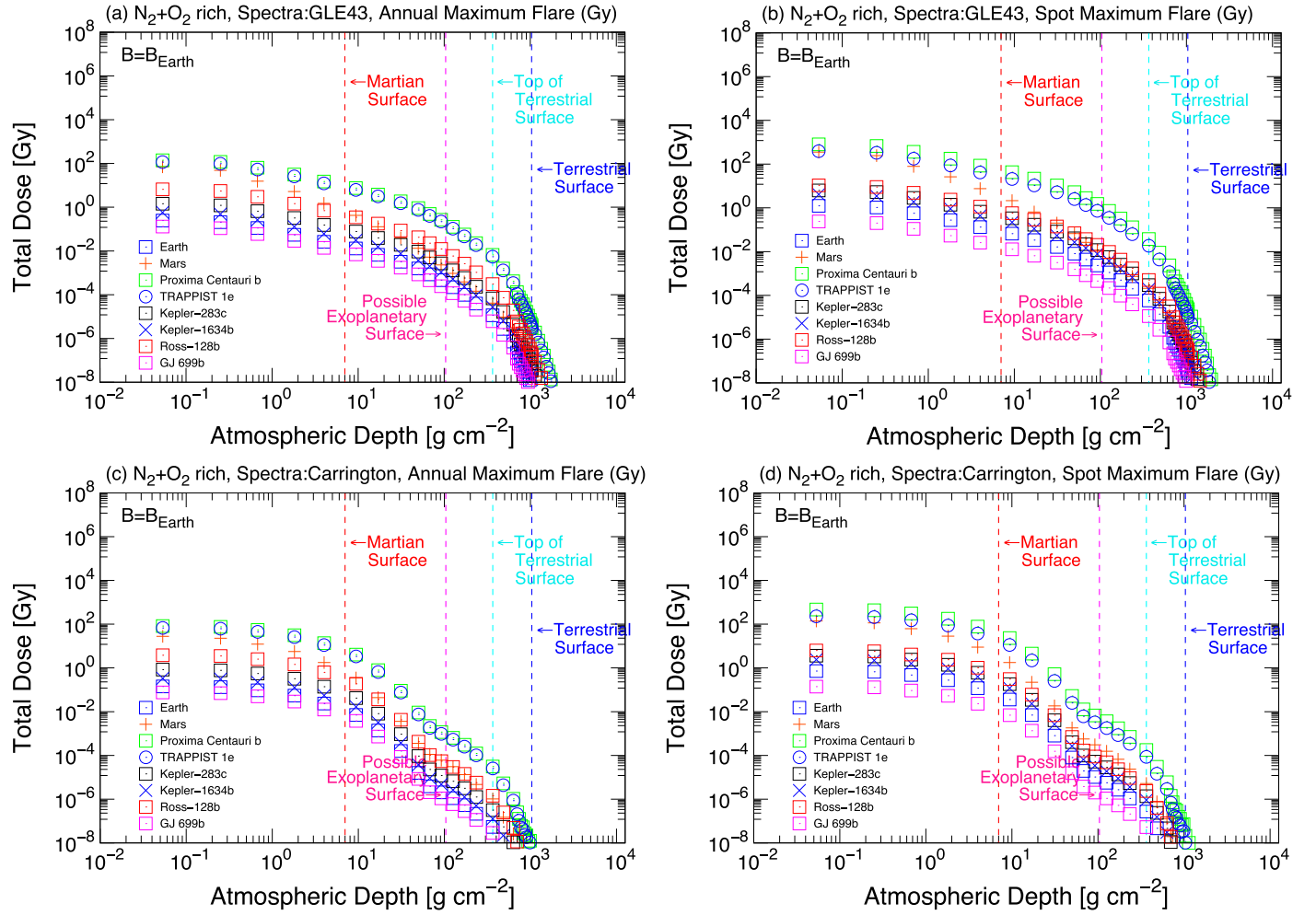


**Figure 15.** Vertical profile of radiation dose (in Sieverts), caused by proton spectrum imitating GLE43 (a and b) and Carrington Flare (c and d) penetrating  $\text{H}_2$ -rich (terrestrial type) atmosphere on Proxima Centauri b (green square), TRAPPIST-1 e (blue circle), Kepler-283 c (brown square), Kepler-1634 b (blue cross), Ross-128 b (red square) and GJ-699 b (pink square) in comparison with the Earth (blue square) and Mars (red plus) in logarithmic scale under annual maximum flare energy (a and c) and under spot maximum flare energy (b and d), in grays. Martian surface atmospheric pressure is equivalent to  $9 \text{ g cm}^{-2}$ ; terrestrial minimum atmospheric pressure, observed at the summit of the Himalayas, is equivalent to  $365 \text{ g cm}^{-2}$ ; (Earth's) ground-level atmospheric pressure is equivalent to  $1037 \text{ g cm}^{-2}$ ; possible exoplanetary surface is one-tenth of terrestrial surface, equivalent to  $103.7 \text{ g cm}^{-2}$ .

observations, is currently only at a hypothetical stage, especially for cool M dwarfs. The specific relationship should be investigated in detail in accordance with photospheric temperature and wavelength. In short, we have to investigate each stellar temperature (spectral class) and planetary body in more detail to clarify those relationships. (3) In general, there are no sufficient observational results about stellar activities especially for active M dwarfs, which should be the focus of future observations. (4) We need to deepen the survey for active M dwarfs when collecting more UV-EUV data, as most stellar objects determined by the MUSCLES survey are not active M dwarfs, except for Proxima Centauri. Moreover, as for Proxima Centauri (Wargelin et al. 2017), the stellar activity may change in accordance with the stellar cycle. (5) We made the first assumption of the ratio for XUV and EUV in this survey, which should be supported and adopted through sufficient observational results. The Mega-MUSCLES project (Froning et al. 2018) will also focus on a survey for TRAPPIST-1, with which we can check the validity of our assumption.

## 5. Conclusion

Our results suggest that both SPE and XUV flux doses are significantly higher at their TOA of close-in exoplanets around M dwarfs than those at Earth. For an exoplanet with a thick atmosphere (with an ozone layer for UV dose), the above extreme fluxes do not affect the dose of ionizing radiation at the planetary surface. When a strong planetary magnetic field is not present or a stellar driver (stellar wind or a CME) is strong enough to perturb the global field and induce strong ionospheric currents that can dissipate into the heat (Cohen et al. 2014; Airapetian et al. 2017b), large XUV fluxes and massive winds can thus affect the erosion of the atmosphere, reducing its thickness on geological timescales (Airapetian et al. 2017b; Garcia-Sage et al. 2017). Accordingly, if the ozone layer is efficiently destroyed by SEP events and the exoplanetary atmosphere is eroded via atmospheric escape (Segura et al. 2010; Airapetian et al. 2017a; Tilley et al. 2019), then stellar XUV emission can penetrate into the planetary surface and provide detrimental conditions to complex life-forms.



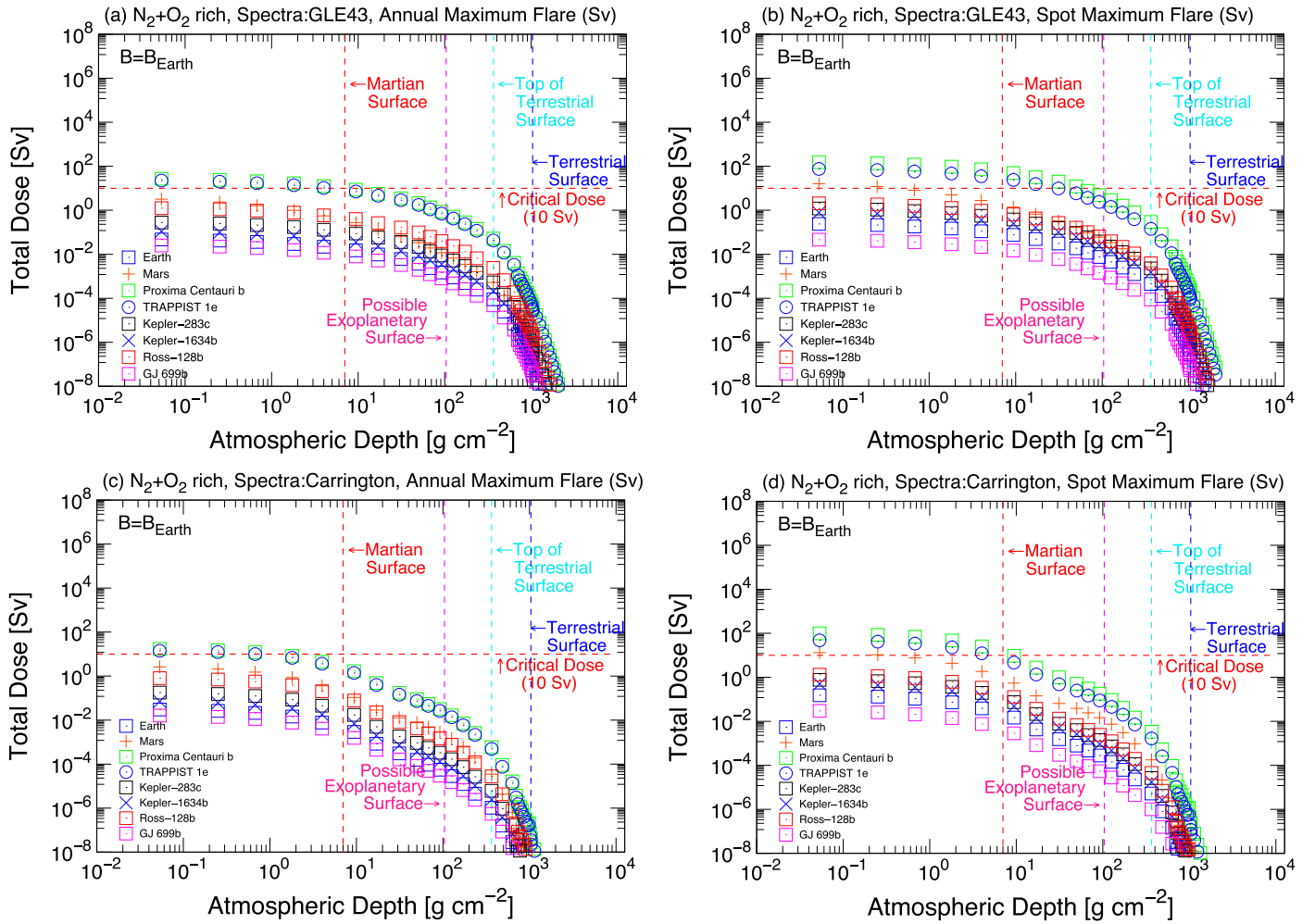


**Figure 16.** Vertical profile of radiation dose (in Sieverts), caused by proton spectrum imitating GLE43 (a and b) and Carrington flare (c and d) penetrating  $\text{H}_2$ -rich (terrestrial type) atmosphere on Proxima Centauri b (green square), TRAPPIST-1 e (blue circle), Kepler-283 c (brown square), Kepler-1634 b (blue cross), Ross-128 b (red square), and GJ-699 b (pink square) in comparison with the Earth (blue square) and Mars (red plus) in logarithmic scale under annual maximum flare energy (a and c) and under spot maximum flare energy (b and d), in Sieverts. Martian surface atmospheric pressure is equivalent to  $9 \text{ g cm}^{-2}$ ; terrestrial minimum atmospheric pressure, observed at the summit of the Himalayas, is equivalent to  $365 \text{ g cm}^{-2}$ ; (Earth's) ground-level atmospheric pressure is equivalent to  $1037 \text{ g cm}^{-2}$ ; possible exoplanetary surface is one-tenth of the terrestrial surface, equivalent to  $103.7 \text{ g cm}^{-2}$ .

According to our scenario, if the atmospheric depth is  $<1/10$  of the terrestrial one, radiation doses become fatal for Proxima Centauri b and TRAPPIST-1 e even under annual maximum flare. Our new proposed scenario also suggests that under high energy and frequency of stellar flares, we can expect that the impact of ionizing radiation on terrestrial-type life-forms is not critical for their evolution if the atmosphere is thick enough ( $\approx 1$  bar). Further efforts should explore the conditions for efficient removal of the UV protection layer (the ozone layer) that reduces the annual UV dose. In this work, we developed a universal estimation method of the stellar flare frequency based on the star spot area observed on each host star. The stellar flare frequency varies from annual maximum flare, 10 yr flare, and possible maximum energy from the star. These estimations were based on Maehara et al. (2017) and Shibata et al. (2013).

Our study indicates that for most “habitable” planets orbiting M-class stars, the radiation dose at the TOA caused by periodic solar superflare activity is far in excess of the critical threshold for terrestrial life to survive. However, the simulations also indicate that planets with sufficient atmospheric thickness and

density ( $\text{N}_2 + \text{O}_2$ ,  $\text{CO}_2$ , and  $\text{H}_2$ ) are, at their crustal surfaces, protectively buffered from the radiation flux arriving at the TOA due to atmospheric attenuation of the incident radiation. This supports the hypothesis of Proxima Centauri b as a habitable planet once it was discovered, even though it is located very close to its host star. In some cases, the incident dose may be reduced sufficiently to support surface life, and this is most notable for atmospheric systems containing significant  $\text{H}_2$ , which would be more common for planets larger than Earth.

In cases where atmospheric thickness alone is not sufficient to attenuate the radiation from solar superflares to non-life-threatening levels, the enhanced attenuation efficacy presented by oceanic bodies may prove critical in preserving marine but not land-based life-forms. The critical atmospheric depth for each planet to secure terrestrial-type life-form evolution on the surface of each planet is  $2.14 \times 10^2 \text{ g cm}^{-2}$  for the Proxima Centauri b,  $4.68 \times 10 \text{ g cm}^{-2}$  for the Ross 128 b, and  $2.04 \times 10^2 \text{ g cm}^{-2}$  for the TRAPPIST-1 e. If we set the critical dose as 1 mSv per year, the critical atmospheric depth becomes  $1.05 \times$

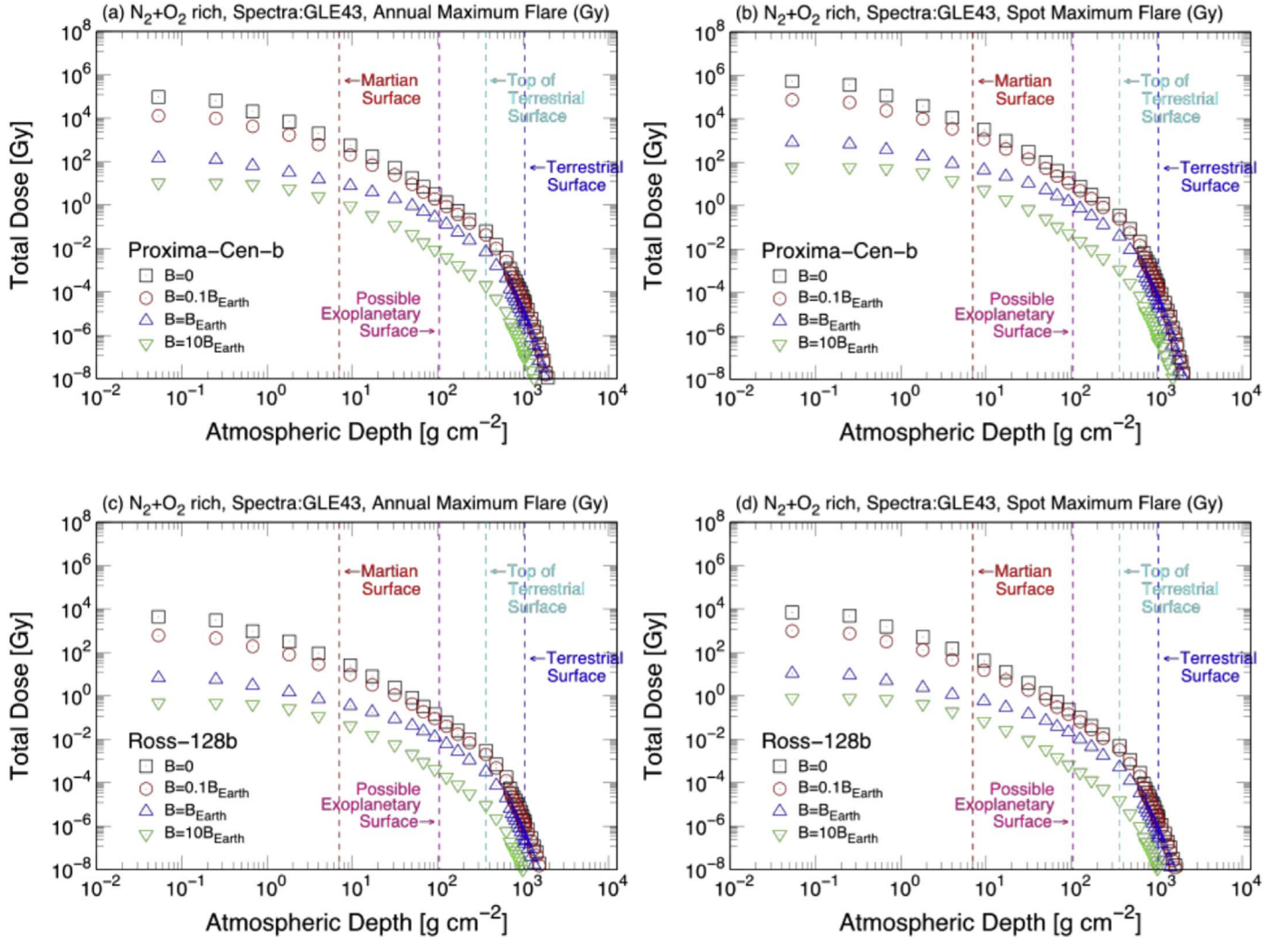


**Figure 17.** Vertical distribution of each radiation dose (in grays) under different magnetic shower caused by SPE air shower penetrating N<sub>2</sub> + O<sub>2</sub>-rich (terrestrial type) on Proxima Centauri b (a and b) and on Ross 128 b (c and d) in logarithmic scale under annual maximum flare energy (a and c) and under spot maximum flare energy calculated by Shibata et al. (2013) (b and d). Martian surface atmospheric pressure is equivalent to 9 g cm<sup>-2</sup>; terrestrial minimum atmospheric pressure, observed at the summit of the Himalayas, is equivalent to 365 g cm<sup>-2</sup>; (Earth's) ground-level atmospheric pressure is equivalent to 1037 g cm<sup>-2</sup>; possible exoplanetary surface is one-tenth of terrestrial surface, equivalent to 103.7 g cm<sup>-2</sup>.

10<sup>3</sup> g cm<sup>-2</sup> for the Proxima Centauri b,  $7.8 \times 10^2$  g cm<sup>-2</sup> for the Ross 128 b, and  $1.04 \times 10^3$  g cm<sup>-2</sup> for the TRAPPIST-1 e.

Do stellar flares present a common life-limiting factor for the development of complex life-forms throughout the universe? Our simulations certainly suggest this might be the case, but equally, for close-in exoplanets around M-type stars that have no substantial atmosphere due to lack of degassing (from volcano-tectonic activity), the atmospheric depth might be insufficient to support terrestrial-type life in the first place, regardless of the periodic sterilizing effect of solar flares.

Future galactic surveys of extrasolar planets aimed at determining habitable planets should characterize stellar activity as part of the analysis process and couple this with assessments of atmospheric composition, the presence of liquid water, and the rate of planetary rotation versus superflare duration. Indications of liquid water on any exoplanet surface, especially oceanic bodies, will likely be a critical indicator for habitability due to the effective protection it provides from solar radiation.

The authors express their sincere thanks to Astronomical Observatory, Kyoto University, and NASA/GSFC for providing us relevant useful data sets and advice. The authors also express their sincere thanks to Professor Takao Doi, Unit of the Synergetic Studies for Space, Kyoto University, for his support for ExoKyoto and observation projects, together with his sincere encouragement for our survey. Special thanks to Ms. Mayumi Tatsuda, secretary, and Ms. Nami Kimura, graduate student, of Earth and Planetary Water Resources Assessment Laboratory, Graduate School of Advanced Integrated Studies in Human Survivability, for her support during the compilation of the whole survey. This work was also supported by JSPS KAKENHI grant Nos. JP16J00320, JP16J06887, JP16H03955, JP17H02865, JP17K05400, JP18J20048, and JP18H01569 and MEXT grant No. 26106006. Yuta Notsu and Shota Notsu are supported by JSPS Overseas Research Fellowship Program. Vladimir Airapetian was supported by NASA grant 80NSSC17K0463, TESS Cycle 1 grant 80NSSC19K0381, and NASA/GSFC ISFM SEEC grant.

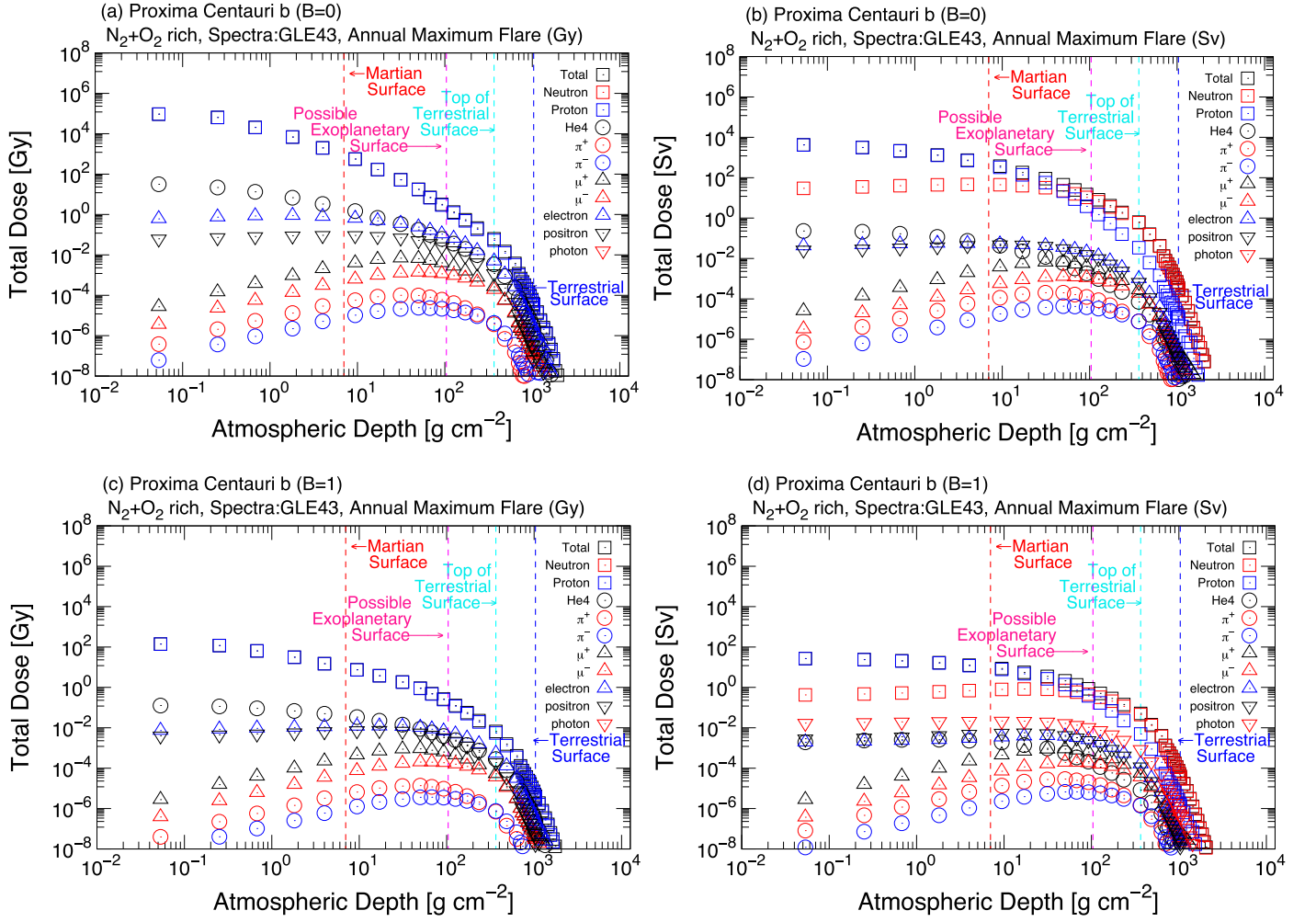


**Figure 18.** Vertical profile of radiation dose in grays and Sieverts, caused by SPE air shower penetrating  $\text{N}_2 + \text{O}_2$ -rich (terrestrial type) atmosphere on Proxima Centauri b with  $B = 0$  (a), (b) and with  $B = B_{\text{Earth}}$  (c and d) under annual maximum flare energy in grays (a and c) and Sieverts (b and d). Martian surface atmospheric pressure is equivalent to  $9 \text{ g cm}^{-2}$ ; terrestrial minimum atmospheric pressure, observed at the summit of the Himalayas, is equivalent to  $365 \text{ g cm}^{-2}$ ; (Earth's) ground-level atmospheric pressure is equivalent to  $1037 \text{ g cm}^{-2}$ ; possible exoplanetary surface is one-tenth of terrestrial surface, equivalent to  $103.7 \text{ g cm}^{-2}$ .

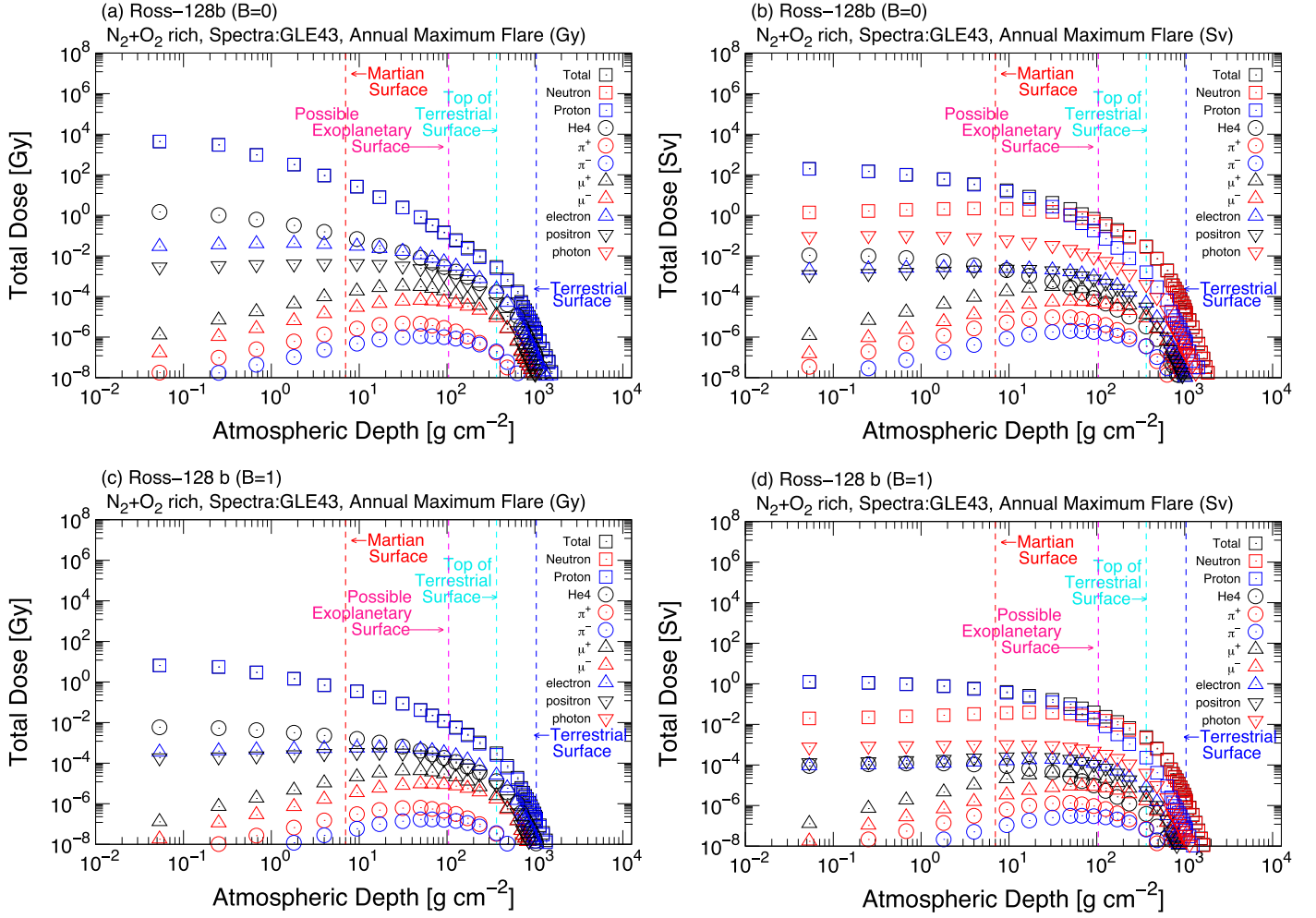


**Figure 19.** Vertical profile of radiation dose in grays and Sieverts, caused by SPE air shower penetrating  $N_2 + O_2$ -rich (terrestrial type) atmosphere on Ross-128 b with  $B = 0$  (a and b) and with  $B = B_{\text{Earth}}$  (c and d) under annual maximum flare energy in grays (a and c) and Sieverts (b and d). Martian surface atmospheric pressure is equivalent to  $9 \text{ g cm}^{-2}$ ; terrestrial minimum atmospheric pressure, observed at the summit of the Himalayas, is equivalent to  $365 \text{ g cm}^{-2}$ ; (Earth's) ground-level atmospheric pressure is equivalent to  $1037 \text{ g cm}^{-2}$ ; possible exoplanetary surface is one-tenth of terrestrial surface, equivalent to  $103.7 \text{ g cm}^{-2}$ .

## Appendix Method

### A.1. Radiation Dose

As mentioned above, two types of radiation doses, the absorbed dose in grays and the effective dose in Sieverts, were deduced from the simulation. In general, the absorbed doses are higher than the effective doses at the TOA because lower energy protons, which have a small impact on the human body due to their shorter range, predominantly contribute to the dose at the location. In contrast, the relation is reversed at the ground level because of the contribution of neutrons, which have a more significant impact on the human body and become very important in such deeper locations.

In this study, we need to presume the critical dose for discussing the habitability of a planet. In general, mortality due to radiation exposure is discussed with respect to the absorbed dose throughout the whole body; for example, the whole-body absorbed dose that is lethal for half of the exposed individuals,  $LD_{50}$ , is around  $4 \text{ Gy}$  for photon exposure (International Commission on Radiological Protection, 2007). However,  $LD_{50}$  is expected to be different for cosmic-ray exposure due to higher relative biological effectiveness. In addition, the whole-body absorbed dose depends on the size of the creature;

the radiological sensitivities significantly vary with species. Thus, we decided to select the effective dose as an index for discussing habitability because it is the most well-known radiological protection quantity and set the critical dose to  $10 \text{ Sv}$  per annually occurring stellar proton event.

### A.2. Parameters and Equations

A single flare event occurs on the stellar surface, and the energy via electromagnetic wave radiates in all directions, whereas during a proton event, the energy has clear directionality. For the SPEs, the release angle of the proton may be limited within a certain angle from the solar equator. We consider that the total area that may be affected by the SPEs can be expressed as

$$A_{\text{SPE}} = 2\pi R_e \times T_D \times H_{\text{SPE}}, \quad (4)$$

$$T_D = 2R_e \sin \theta_V, \quad (5)$$

$$H_{\text{SPE}} = \frac{\theta_H}{360}, \quad (6)$$

in which  $A_{\text{SPE}}$  is the total flare affected area in  $1 \text{ au}$  distance,  $R_e$  is Earth's semimajor axis,  $H_{\text{SPE}}$  is the ratio of SPE horizontal release angle over the entire orbital circle,  $\theta_V$  is the



**Table 4**  
UV Energy from Annual Maximum Flare at TOA in Each Planet

Exoplanet	$E_{\text{UV}}^{\text{flare a}}$	$\frac{E_{\text{UV}}^{\text{flare b}}}{E_{\text{UV,Earth}}^{\text{flare}}}$	$\frac{E_{\text{UV}}^{\text{flare c}}}{E_{\text{UV,Earth}}^{\text{flux}}}$	$E_{\text{XUV}}^{\text{flare d}}$	$\frac{E_{\text{XUV}}^{\text{flare e}}}{E_{\text{XUV,Earth}}^{\text{flare}}}$	$\frac{E_{\text{XUV}}^{\text{flare f}}}{E_{\text{XUV,Earth}}^{\text{flux}}}$	$E_{\text{XUV}}^{\text{normal g}}$
Name	(J m <sup>-2</sup> )		(%)	(J m <sup>-2</sup> )		(%)	(J m <sup>-2</sup> )
GJ 699 b	8.74E+03	7.27E+04	2.59E-06	4.37E+03	7.27E+04	2.51E-02	2.35E+04
Kepler-283 c	4.43E+02	3.69E+03	1.31E-07	2.22E+02	3.69E+03	1.27E-03	1.19E+06
Kepler-1634 b	4.60E+04	3.83E+05	1.37E-05	2.30E+04	3.83E+05	1.32E-01	6.67E+05
Proxima Centauri b	1.57E+04	1.31E+05	4.66E-06	7.86E+03	1.31E+05	4.51E-02	1.33E+07
Ross-128 b	8.75E+04	7.28E+05	2.60E-05	4.38E+04	7.28E+05	2.51E-01	1.38E+06
TRAPPIST-1 b	5.30E+04	4.41E+05	1.57E-05	2.65E+04	4.41E+05	1.52E-01	5.99E+07
TRAPPIST-1 c	2.82E+04	2.35E+05	8.39E-06	1.41E+04	2.35E+05	8.11E-02	3.20E+07
TRAPPIST-1 d	1.42E+04	1.18E+05	4.22E-06	7.12E+03	1.18E+05	4.08E-02	1.61E+07
TRAPPIST-1 e	8.24E+03	6.86E+04	2.45E-06	4.12E+03	6.86E+04	2.37E-02	9.32E+06
TRAPPIST-1 f	4.75E+03	3.96E+04	1.41E-06	2.38E+03	3.96E+04	1.36E-02	5.38E+06
TRAPPIST-1 g	3.22E+03	2.68E+04	9.54E-07	1.61E+03	2.68E+04	9.23E-03	3.64E+06
TRAPPIST-1 h	1.65E+03	1.37E+04	4.89E-07	8.24E+02	1.37E+04	4.73E-03	1.86E+06
Sol d (Earth)	3.70E-01	3.08E+00	1.10E-10	1.85E-01	3.08E+00	1.06E-06	1.74E+05
Sol e (Mars)	1.59E-01	1.33E+00	4.72E-11	7.96E-02	1.33E+00	4.57E-07	7.51E+04
Exoplanet	$E_{\text{UV}}^{\text{normal h}}$	$E_{\text{Visible}}^{\text{normal i}}$	$E_{\text{IR}}^{\text{normal j}}$	$E_{\text{XUV}}^{\text{flare+quiescent k}}$	$\frac{E_{\text{XUV}}^{\text{flare+quiescent l}}}{E_{\text{XUV,Earth}}^{\text{flare+quiescent}}}$	$E_{\text{UV}}^{\text{flare+quiescent m}}$	$\frac{E_{\text{UV}}^{\text{flare+quiescent n}}}{E_{\text{UV,Earth}}^{\text{flare+quiescent}}}$
Name	(J m <sup>-2</sup> )	(J m <sup>-2</sup> )	(J m <sup>-2</sup> )	(J m <sup>-2</sup> )		(J m <sup>-2</sup> ) <sup>l</sup>	
GJ 699 b	1.65E+06	8.68E+07	7.79E+08	2.79E+04	0.16	1.66E+06	0.00
Kepler-283 c	4.25E+08	1.14E+10	2.83E+10	1.19E+06	6.82	4.25E+08	0.13
Kepler-1634 b	1.79E+09	1.14E+10	1.33E+10	6.90E+05	3.96	1.79E+09	0.53
Proxima Centauri b	2.44E+07	8.78E+08	2.74E+10	1.33E+07	76.21	2.44E+07	0.01
Ross-128 b	9.25E+07	5.01E+09	5.81E+10	1.50E+06	8.61	9.25E+07	0.03
TRAPPIST-1 b	2.13E+08	8.97E+09	1.72E+11	7.29E+07	418.36	2.13E+08	0.06
TRAPPIST-1 c	1.14E+08	4.79E+09	9.19E+10	3.89E+07	223.21	1.14E+08	0.03
TRAPPIST-1 d	5.73E+07	2.41E+09	4.63E+10	1.96E+07	112.34	5.73E+07	0.02
TRAPPIST-1 e	3.32E+07	1.40E+09	2.68E+10	1.13E+07	65.07	3.32E+07	0.01
TRAPPIST-1 f	1.91E+07	8.05E+08	1.54E+10	6.54E+06	37.52	1.91E+07	0.01
TRAPPIST-1 g	1.30E+07	5.44E+08	1.05E+10	4.42E+06	25.39	1.30E+07	0.00
TRAPPIST-1 h	6.64E+06	2.79E+08	5.36E+09	2.27E+06	13.01	6.64E+06	0.00
Sol d (Earth)	3.37E+09	1.93E+10	2.04E+10	1.74E+05	1.00	3.37E+09	1.00
Sol e (Mars)	1.45E+09	8.32E+09	8.81E+09	7.51E+04	0.43	1.45E+09	0.43

**Notes.** TOA  $\approx 0$  g cm<sup>-2</sup>.

<sup>a</sup> UV energy by annual maximum flare at TOA.

<sup>b</sup> Ratio to Earth's annual maximum flare.

<sup>c</sup> Ratio to Earth's annual UV flux at TOA.

<sup>d</sup> XUV energy by annual maximum flare at TOA.

<sup>e</sup> Ratio to Earth's annual maximum flare.

<sup>f</sup> Ratio to Earth's annual UV flux at TOA.

<sup>g</sup> Annual XUV energy by normal stellar radiation at TOA.

<sup>h</sup> Annual UV energy by normal stellar radiation at TOA.

<sup>i</sup> Annual visible ray energy by normal stellar radiation at TOA.

<sup>j</sup> Annual IR energy by normal stellar radiation at TOA.

<sup>k</sup> Annual total (flare + quiescent) XUV energy at TOA.

<sup>l</sup> Ratio to Earth/annual total (flare + quiescent) XUV energy at TOA.

<sup>m</sup> Annual total (flare + quiescent) UV energy at TOA.

<sup>n</sup> Ratio to Earth/annual total (flare + quiescent) UV energy at TOA.

vertical release angle of SPEs, and  $\theta_H$  is the horizontal release angle of SPE (in this study we assume that  $\theta_V$  and  $\theta_H$  are equal to 15° and 90°, respectively).

Thus, the expected SPE energy per unit area received at Earth's TOA during a determined period (1 yr) can be expressed as

$$E_{\text{SPE,Earth}} = \frac{E_{\text{flare}} \times H_P \times R_{\text{SPE}}}{A_{\text{SPE}}}, \quad (7)$$

in which  $H_P = \theta_H/180$  is the horizontal exposure probability (we employ 0.5) and  $R_{\text{SPE}}$  is the fraction of SPE energy in total

flare energy per year. In this study, we employed 0.25 (Aschwanden et al. 2017).

From the above equation, we may calculate fluence on any exoplanet using the relative proportion to the fluence at Earth's TOA.

### A.3. Normalization

In order to apply this comparison with stellar flares, we employed a normalized value based on the *GOES* X-ray class of the flare events. We can safely assume that total energy of flares can be estimated from the *GOES* X-ray class

**Table 5**  
UV Energy at TOA, with Synthesized Spectra Assuming 100% of the Impact Ratio of Star Spot in Equation (10)

Exoplanet	$E_{\text{UV}}^{\text{flare a}}$	$\frac{E_{\text{UV}}^{\text{flare b}}}{E_{\text{UV,Earth}}^{\text{flare}}}$	$\frac{E_{\text{UV}}^{\text{flare c}}}{E_{\text{flux,Earth}}^{\text{flare}}}$	$E_{\text{XUV}}^{\text{flare d}}$	$\frac{E_{\text{XUV}}^{\text{flare e}}}{E_{\text{XUV,Earth}}^{\text{flare}}}$	$\frac{E_{\text{XUV}}^{\text{flare f}}}{E_{\text{flux,Earth}}^{\text{flare}}}$	$E_{\text{XUV}}^{\text{normal g}}$
Name	(J m <sup>-2</sup> )		(%)	(J m <sup>-2</sup> )		(%)	(J m <sup>-2</sup> )
Kepler-283 c	8.24E+03	6.85E+04	2.44E-06	4.12E+03	6.85E+04	2.36E-02	1.01E+05
Kepler-1634 b	4.60E+04	3.83E+05	1.37E-05	2.30E+04	3.83E+05	1.32E-01	7.07E+05
Proxima Centauri b	1.57E+04	1.31E+05	4.66E-06	7.86E+04	1.31E+05	4.51E-02	1.33E+07
Ross-128 b	8.75E+04	7.28E+05	2.60E-05	4.38E+04	7.28E+05	2.51E-01	1.38E+06
TRAPPIST-1 b	5.30E+04	4.41E+05	1.57E-05	2.65E+04	4.41E+05	1.52E-01	1.12E+08
TRAPPIST-1 c	2.83E+04	2.35E+05	8.39E-06	1.41E+04	2.35E+05	8.11E-02	5.99E+07
TRAPPIST-1 d	1.42E+04	1.18E+05	4.22E-06	7.12E+03	1.18E+05	4.08E-02	3.01E+07
TRAPPIST-1 e	8.24E+03	6.86E+04	2.45E-06	4.12E+03	6.86E+04	2.37E-02	1.75E+07
TRAPPIST-1 f	4.75E+03	3.96E+04	1.41E-06	2.38E+03	3.96E+04	1.36E-02	1.01E+07
TRAPPIST-1 g	3.22E+03	2.68E+04	9.54E-07	1.61E+03	2.68E+04	9.23E-03	6.81E+06
TRAPPIST-1 h	1.65E+03	1.37E+04	4.89E-07	8.24E+02	1.37E+04	4.73E-03	3.49E+06
Sol d (Earth)	3.70E-01	3.08E+00	1.10E-10	1.85E-01	3.08E+00	1.06E-06	1.74E+05
Sol e (Mars)	1.60E-01	1.33E+00	4.72E-11	7.96E-02	1.33E+00	4.57E-07	7.51E+04
Exoplanet	$E_{\text{UV}}^{\text{normal h}}$	$E_{\text{Visible}}^{\text{normal i}}$	$E_{\text{IR}}^{\text{normal j}}$	$E_{\text{XUV}}^{\text{flare+quiescent k}}$	$\frac{E_{\text{XUV}}^{\text{flare+quiescent l}}}{E_{\text{XUV,Earth}}^{\text{flare+quiescent}}}$	$E_{\text{UV}}^{\text{flare+quiescent m}}$	$\frac{E_{\text{UV}}^{\text{flare+quiescent n}}}{E_{\text{UV,Earth}}^{\text{flare+quiescent}}}$
Name	(J m <sup>-2</sup> )	(J m <sup>-2</sup> )	(J m <sup>-2</sup> )	(J m <sup>-2</sup> )		(J m <sup>-2</sup> )	
Kepler-283 c	1.96E+09	1.12E+10	1.19E+10	1.05E+05	0.60	1.96E+09	0.58
Kepler-1634 b	1.90E+09	1.21E+10	1.41E+10	7.30E+03	4.19	1.90E+09	0.56
Proxima Centauri b	2.44E+07	8.78E+08	2.74E+10	1.33E+07	76.21	2.44E+07	0.01
Ross-128 b	9.24E+07	5.01E+09	5.81E+10	1.42E+06	8.17	9.25E+07	0.03
TRAPPIST-1 b	2.53E+08	8.97E+09	1.72E+11	1.12E+08	644.10	2.53E+08	0.07
TRAPPIST-1 c	1.35E+08	4.79E+09	9.19E+10	5.99E+07	343.66	1.35E+08	0.04
TRAPPIST-1 d	6.79E+07	2.41E+09	4.63E+10	3.01E+07	172.95	6.79E+07	0.02
TRAPPIST-1 e	3.93E+07	1.40E+09	2.68E+10	1.75E+07	100.19	3.97E+07	0.01
TRAPPIST-1 f	2.27E+07	8.04E+08	1.54E+10	1.01E+07	57.76	2.27E+07	0.01
TRAPPIST-1 g	1.53E+07	5.44E+08	1.05E+10	6.81E+06	39.09	1.53E+07	0.00
TRAPPIST-1 h	7.86E+06	2.79E+08	5.36E+09	3.49E+06	20.03	7.86E+06	0.00
Sol d (Earth)	3.37E+09	1.93E+10	2.04E+10	1.74E+05	1.00	3.37E+09	1.00
Sol e (Mars)	1.45E+09	8.32E+09	8.81E+09	750E+04	0.43	1.45E+09	0.43

**Notes.** TOA  $\approx 0 \text{ g cm}^{-2}$ .

<sup>a</sup> UV energy by annual maximum flare at TOA.

<sup>b</sup> Ratio to Earth's annual maximum flare.

<sup>c</sup> Ratio to Earth's annual UV flux at TOA.

<sup>d</sup> XUV energy by annual maximum flare at TOA.

<sup>e</sup> Ratio to Earth's annual maximum flare.

<sup>f</sup> Ratio to Earth's annual UV flux at TOA.

<sup>g</sup> Annual XUV energy by normal stellar radiation at TOA.

<sup>h</sup> Annual UV energy by normal stellar radiation at TOA.

<sup>i</sup> Annual visible ray energy by normal stellar radiation at TOA.

<sup>j</sup> Annual IR energy by normal stellar radiation at TOA.

<sup>k</sup> Annual total (flare + quiescent) XUV energy at TOA.

<sup>l</sup> Ratio to Earth/annual total (flare + quiescent) XUV energy at TOA.

<sup>m</sup> Annual total (flare + quiescent) UV energy at TOA.

<sup>n</sup> Ratio to Earth of annual total (flare + quiescent) UV energy at TOA.

(Namekata et al. 2017). Accordingly, we assumed that the total energy of the Carrington-class event (estimated as X45 class) was  $4.5 \times 10^{25}$  Joules and GLE43 (estimated as X13 class) was  $1.3 \times 10^{25}$  Joules.

To integrate the above reference of SPEs, applicable for stellar proton events, the following constants are determined as

$$E_{\text{PEGLE43}} = \frac{E_{\text{GLE43}} \times R_{\text{SPE}}}{A_{\text{SPE}}}, \quad (8)$$

$$E_{\text{PECar}} = \frac{E_{\text{Car}} \times R_{\text{SPE}}}{A_{\text{SPE}}}, \quad (9)$$

in which  $E_{\text{GLE43}}$  is the total energy of GLE43 (estimated as  $1.3 \times 10^{32} \text{ [erg]} = 1.3 \times 10^{25} \text{ [Joule]}$ ) and  $E_{\text{Car}}$  is the total energy of a Carrington-class event (estimated as  $4.5 \times 10^{32} \text{ [erg]} = 1.3 \times 10^{25} \text{ [Joule]}$ ). Note that coefficient  $H_p$  has not been multiplied as it is obvious that those events released SEP toward the Earth.

#### A.4. XUV Radiation

XUV radiation is considered one type of harmful radiation released from a single stellar flare event. The proportion of XUV radiation in a single flare event has not been fully

determined. However, according to Aschwanden et al. (2017), the energetic portion of the UV continuum (with the sum of the ranges 200–228, 370–504, 504–912, 1464–1609, and 1600–1740 Å) is  $3.96 \times 10^{29}$  erg, equivalent to 1.8% of estimated total flare energy (X2.2 class event  $2.2 \times 10^{31}$  erg) in a solar flare. In this study, since there are no related studies about the proportion of UV radiation as a function of stellar temperature, diameter, and other factors, we use solar flare results (Aschwanden et al. 2017) as a reference and roughly assume that the UV portion of 10% of total flare energy is the most extreme case. To determine the portion of XUV in the total UV dose of the flare as one extreme case, we assume that 50% of the total UV energy emitted during stellar flare is XUV energy.

When determining normal UV irradiation for each of the exoplanets, since there are no direct observations for most of the target stars, we synthesize the spectra using the published spectra curve from the MUSCLES project (France et al. 2016; Loyd et al. 2016; Youngblood et al. 2016) (using dapt-const-res-sed SED in version 2.2 data set) and applied a similar spectral on the basis of temperature, trying to create an extreme UV case of a similar type to the star. We used the MUSCLES-observed spectra for 13 stars (GJ1214, GJ551 [Proxima Cen], GJ876, GJ436, GJ581, GJ667C, GJ176, GJ832, HD 85512, HD 40307, HD 97658, eps Eridanis, and the Sun) and synthesized the spectra for the target stars (TRAPPIST-1, Ross-128, Kepler-283, Kepler-1634). In the synthesizing process we divide the whole spectra into two, (1) one that is mostly related to the photospheric temperature, applied for IR, VR, and UVA and UVB, in particular for wavelengths longer than 1200 Å; and (2) one that is mostly related to the magnetic activity mainly in the chromosphere, applied for XUV, in particular for the wavelength from 1 to 1200 Å. For (2) we made the hypothesis that the intensity of XUV is in proportion to the star spot area, based on the hypothesis that the star spot area represents the average magnetic field strength of the target star, thus the chromospheric activity level. In this study, because our aim is to evaluate extreme cases under different star systems, we introduce a ratio to specify the weight of each effect. Currently, we set two extreme cases when synthesizing the spectra of the XUV portion, as (1) 100% of the total magnetic flux-related (magnetic) term, generated from observed XUV (GJ551) calculated using the relative portion of the star spot area, and (2) 60% of the magnetic term + 40% of the photosphere temperature-related (photospheric) term. We set 20% of the magnetic term + 80% of the photospheric term when synthesizing the spectra of the EUV portion, while applying the following equation to synthesized fluxes in each wavelength:

$$F_I = R_{A_{\text{spotUV}}} \times F_{A_{\text{spot}}} + (1 - R_{A_{\text{spotUV}}})F_{T_{\text{eff}}}, \quad (10)$$

in which  $F_I$  is the UV flux for target stars,  $R_{A_{\text{spotUV}}}$  is the impact ratio of star spot in UV (same for XUV),  $F_{A_{\text{spot}}}$  is the flux calculated from the relative size of the star spot area, normalized by the observed GJ551 (Proxima Cen) star spot area and its UV (XUV) spectra, and  $F_{T_{\text{eff}}}$  is the flux calculated from the photospheric temperature of the star.

For example, when synthesizing a portion of IR, VR, far-FUV, middle-UV, and near-UV for TRAPPIST-1 (2550 K), for the VR, IR region, we employed the spectra of GJ1214 (2935 K) as a proxy for a lower temperature star. The spectra of Ross-128 (3192 K) were computed with GJ876 (3062 K) and



GJ436 (3281 K). The spectra of Kepler-283 (4351 K) were calculated using HD 85512 (4305 K) and HD 40307 (4783 K), and the spectra of Kepler-1634 (5474 K) were synthesized with that of eps Eridanis and our Sun. For the chromospheric component (XUV), we synthesized spectra mainly from Proxima Centauri and eps Eridanis, whose XUV components were much higher than that of other stars.




Then we calculated the portion of UV (including XUV and others) and set its value as the radiation boundary from the central star. Irradiance at the top of the atmosphere of each planet can be calculated using normal radiation propagation. Estimating UV energy from stellar flares, we applied the statistical occurrence probability and possible total energy of the flare from each central star. Applying this UV energy ratio and projected planetary position, we calculated the energy at the TOA of each planet. Using the above hypotheses, the most intensive UV and XUV at the TOA induced by annual maximum flares, assuming this portion, were observed on Ross-128 b, reaching  $8.75 \times 10^5 \text{ J m}^{-2}$  for total UV and  $4.38 \times 10^5 \text{ J m}^{-2}$  for XUV (1–1200 Å), followed by Kepler-1634 b with  $4.60 \times 10^4 \text{ J m}^{-2}$ , Proxima Centauri b with  $1.57 \times 10^4 \text{ J m}^{-2}$ , and TRAPPIST-1 e with  $8.24 \times 10^3 \text{ J m}^{-2}$ , as shown in Table 4. Although all values are largely compared with terrestrial impact values, they are all below 0.001% of the terrestrial annual UV dose at the TOA (estimated as  $4.31 \times 10^9 \text{ J m}^{-2}$ , shown in Table 4). Also, by comparing the total dose during annual irradiation, the total value is far below the annual dose for the terrestrial case. The total annual UV (10–4000 Å) dose does not reach the terrestrial level for all of the exoplanets, with the maximum value 0.53 in the terrestrial case of Kepler-1634 b.

At the same time, limiting the dose of XUV (1–1200 Å), most habitable exoplanets have a higher value compared with that of Earth, reaching up to 76 times the value at Proxima Centauri b, followed by TRAPPIST-1 e with 65 times in the (2) calculation, since the XUV portion in the normal irradiation of the Sun is smaller than the observed M dwarf and thus it reflects an annual dose. On TRAPPIST-1 b, c, and d, the XUV portion reaches a significant value of 418, 223, and 112, respectively (as shown in Table 4). When applying the most extreme cases (1), TRAPPIST-1 e becomes the highest, reaching 100 times the value compared with Earth. On TRAPPIST-1 b, c, and d for the (1) calculation, the XUV portion reaches significant values of 644, 344, and 173 times, respectively (as shown in Table 5). They are, however, generally considered as nonhabitable planets in the system. Having relevant atmospheric depth and an ion layer, equivalent to that of the Earth—where most of XUV is absorbed by a factor of  $10^{-15}$ – $10^{-22}$ , the irradiation may be absorbed before reaching the planetary surface. The flare impact on the UV dose only becomes important when superflares induce a significant reduction of the ozone layer (Segura et al. 2010) or when they accelerate significant atmospheric escape (Airapetian et al. 2016). Accordingly the atmospheric protection becomes more important for those planets due to higher ratio of normal irradiation of XUV.

## ORCID iDs

Yosuke A. Yamashiki  <https://orcid.org/0000-0001-6241-4741>

Hiroyuki Maehara  <https://orcid.org/0000-0003-0332-0811>  
Vladimir Airapetian  <https://orcid.org/0000-0003-4452-0588>

Yuta Notsu  <https://orcid.org/0000-0002-0412-0849>  
 Shota Notsu  <https://orcid.org/0000-0003-2493-912X>  
 Takanori Sasaki  <https://orcid.org/0000-0003-1242-7290>

## References

- Airapetian, V., Barnes, R., Cohen, O., et al. 2019, arXiv:1905.05093  
 Airapetian, V. S., Glocer, A., Gronoff, G., Hébrard, E., & Danchi, W. 2016, *NatGe*, **9**, 452  
 Airapetian, V. S., Glocer, A., Khazanov, G. V., et al. 2017a, *ApJL*, **836**, L3  
 Airapetian, V. S., Jackman, C., Mlynzcak, M., Danchi, W., & Hunt, M. 2017b, *NatSR*, **7**, 14141  
 Aschwanden, M. J., Caspi, A., Cohen, C. M. S., et al. 2017, *ApJ*, **836**, 17  
 Atri, D. 2017, *MNRAS*, **465**, L34  
 Cohen, O., Drake, J. J., Glocer, A., et al. 2014, *ApJ*, **790**, 57  
 Davenport, J. R. A. 2016, *ApJ*, **829**, 23  
 Elkins-Tanton, L. T., & Seager, S. 2008, *ApJ*, **685**, 1237  
 France, K., Loyd, R. O. P., Youngblood, A., et al. 2016, *ApJ*, **820**, 89  
 Froning, C. S., France, K., Loyd, R. O. P., et al. 2018, AAS Meeting, **231**, 111.05  
 Garcia-Sage, K., Glocer, A., Drake, J. J., Gronoff, G., & Cohen, O. 2017, *ApJL*, **844**, L13  
 Gopalswamy, N., Yashiro, S., Akiyama, S., & Xie, H. 2017, *SoPh*, **292**, 65  
 Grießmeier, J.-M., Tabataba-Vakili, F., Stadelmann, A., Grenfell, J. L., & Atri, D. 2015, *A&A*, **581**, A44  
 International Commission on Radiological Protection (ICRP) 2007, ICRP Publication 103 (Ottawa, ON: ICRP)  
 International Commission on Radiological Protection (ICRP) 2010, ICRP Publication 116 (Ottawa, ON: ICRP)  
 Jakosky, B. M., Grebowsky, J. M., Luhmann, J. G., et al. 2015, *Sci*, **350**, 0210  
 Kasting, J. F. 1988, *Icar*, **74**, 472  
 Kasting, J. F., Whitmire, D. P., & Reynolds, R. T. 1993, *Icar*, **101**, 108  
 Kay, C., Opher, M., & Kornbleuth, M. 2016, *ApJ*, **826**, 195  
 Kopparapu, R. K., Ramirez, R., Kasting, J. F., et al. 2013, *ApJ*, **765**, 131  
 Kumari, A., Ramesh, R., Kathiravan, C., & Gopalswamy, N. 2017, *ApJ*, **843**, 10  
 Lammer, H., Zerkle, A. L., Gebauer, S., et al. 2018, *A&ARv*, **26**, 2  
 Lingam, M., & Loeb, A. 2017, *ApJ*, **848**, 41  
 Loyd, R. O. P., France, K., Youngblood, A., et al. 2016, *ApJ*, **824**, 102  
 Maehara, H., Notsu, Y., Notsu, S., et al. 2017, *PASJ*, **69**, 41  
 Maehara, H., Shibayama, T., Notsu, S., et al. 2012, *Natur*, **485**, 478  
 Maehara, H., Shibayama, T., Notsu, Y., et al. 2015, *EP&S*, **67**, 59  
 Miyake, F., Masuda, K., & Nakamura, T. 2013, *NatCo*, **4**, 1748  
 Miyake, F., Nagaya, K., Masuda, K., & Nakamura, T. 2012, *Natur*, **486**, 240  
 Namekata, K., Sakaue, T., Watanabe, K., et al. 2017, *ApJ*, **851**, 91  
 Notsu, Y., Honda, S., Maehara, H., et al. 2015a, *PASJ*, **67**, 32  
 Notsu, Y., Honda, S., Maehara, H., et al. 2015b, *PASJ*, **67**, 33  
 Notsu, Y., Maehara, H., Honda, S., et al. 2019, *ApJ*, **876**, 58  
 Notsu, Y., Shibayama, T., Maehara, H., et al. 2013, *ApJ*, **771**, 127  
 Ramirez, R. M., Abbot, D. S., Fujii, Y., et al. 2019, arXiv:1903.03706  
 Ribas, I., Gregg, M. D., Boyajian, T. S., & Bolmont, E. 2017, *A&A*, **603**, A58  
 Sato, T. 2015, *PLoS*, **10**, e0144679  
 Sato, T., Iwamoto, Y., Hashimoto, S., et al. 2018, *Journal of Nuclear Science and Technology*, **55**, 684  
 Sato, T., Kataoka, R., Shiota, D., et al. 2018, *SpWea*, **16**, 924  
 Sato, T., Kataoka, R., Yasuda, H., et al. 2014, *Radiation Protection Dosimetry*, **161**, 274  
 Schrijver, C. J., Kauristie, K., Aylward, A. D., et al. 2015, *AdSpR*, **55**, 2745  
 Segura, A., Walkowicz, L. M., Meadows, V., Kasting, J., & Hawley, S. 2010, *AsBio*, **10**, 751  
 Shibata, K., Isobe, H., Hillier, A., et al. 2013, *PASJ*, **65**, 49  
 Shibayama, T., Maehara, H., Notsu, S., et al. 2013, *ApJS*, **209**, 5  
 Smart, D. F., Shea, M. A., & McCracken, K. G. 2006, *AdSpR*, **38**, 215  
 Takahashi, T., Mizuno, Y., & Shibata, K. 2016, *ApJL*, **833**, L8  
 Tilley, M. A., Segura, A., Meadows, V., Hawley, S., & Davenport, J. 2019, *AsBio*, **19**, 64  
 Townsend, L. W., Stephens, D. L., Hoff, J. L., et al. 2006, *AdSpR*, **38**, 226  
 Usoskin, I. G., Kromer, B., Ludlow, F., et al. 2013, *A&A*, **552**, L3  
 Wargelin, B. J., Saar, S. H., Pojmański, G., Drake, J. J., & Kashyap, V. L. 2017, *MNRAS*, **464**, 3281  
 Xapsos, M. A., Barth, J. L., Stassinopoulos, E., et al. 2000, *ITNS*, **47**, 2218  
 Youngblood, A., France, K., Loyd, R. O. P., et al. 2016, *ApJ*, **824**, 101